Liang, J.; Guo, Y.; Richter, N.; Xie, H.; Vachula, R.S.; Lupien, R.L.; Zhao, B.; Wang, M.; Yao, Y.; Hou, J.; Liu, J.; Russell, J.M. (2022). Calibration and application of branched GDGTs to Tibetan lake sediments: The influence of temperature on the fall of the Guge Kingdom in Western Tibet, China. *Paleoceanography and Paleoclimatology 37(5)*: e2021PA004393. DOI: 10.1029/2021pa004393

Published version: https://dx.doi.org/10.1029/2021pa004393

NIOZ Repository: http://imis.nioz.nl/imis.php?module=ref&refid=352832

Calibration and application of branched GDGTs to Tibetan lake sediments: the influence of temperature on the fall of the Guge Kingdom in Western Tibet, China

Jie Liang[1,2*], Yanlong Guo[3], Nora Richter[4], Haichao Xie[1*], Richard S. Vachula[5], Rachel L. Lupien[6], Boyang Zhao[2], Mingda Wang[7], Yuan Yao[8], Juzhi Hou[1], Jianbao Liu[1], James M. Russell[2]

1. Group of Alpine Paleoecology and Human Adaptation (ALPHA), State Key Laboratory of Tibetan Plateau Earth System, Resources and Environment (TPESRE), Institute of Tibetan Plateau Research, Chinese Academy of Sciences, Beijing 100101, China
2. Department of Earth, Environmental, and Planetary Sciences, Brown University, Providence 02912, USA
3. National Tibetan Plateau Data Center, Key Laboratory of Tibetan Environmental Changes and Land Surface Processes, Institute of Tibetan Plateau Research, Beijing 100101, China
4. NIOZ Royal Institute for Sea Research, Department of Marine Microbiology and Biogeochemistry, P.O. Box 59, 1790 AB Den Burg, Texel, The Netherlands
5. Department of Geology, College of William and Mary, Williamsburg 23185, USA
6. Division of Biology and Paleo Environment, Lamont-Doherty Earth Observatory, Palisades 10964, USA
7. School of Geography, Liaoning Normal University, Dalian 116029, China
8. Institute of Global Environmental Change, Xi’an Jiaotong University, Xi’an 710054, China

*Corresponding authors：

liangjie@itpcas.ac.cn

hcxie@itpcas.ac.cn

Key points

1. Different lake mixing types profoundly impact brGDGT-reconstructed temperatures.
2. Air temperatures in Western Tibet were 2 – 3 °C cooler than present during the LIA.
3. Temperature variability influenced crop yield. A decreased crop yield likely contributed to the collapse of the Guge Kingdom.

Abstract

Branched glycerol dialkyl glycerol tetraethers (brGDGTs) from lacustrine sediments have been widely used to reconstruct mean annual air temperature (MAAT). Although many proxy calibrations relating brGDGT characteristics have been put forth, these calibrations may produce warm biases when applied to lakes in cold regions. We present an expanded Chinese lake surface sediment brGDGT-MAAT calibration with 29 new surface samples from cold regions along with 39 previously published from Chinese lakes. We deployed sediment traps in a meromictic lake, Dagze Co, and compared results with previously published data from a dimictic lake, Lake 578 in Greenland, to determine potential seasonal and depth-dependence of brGDGTs. In the meromictic lake, brGDGTs are primarily produced in the lake bottom water, whereas in the dimictic lake the brGDGTs are produced throughout the water column and mainly reflect the annual bottom water temperature or mixing season water column temperature. We applied our refined calibration to a sediment core from Western Tibet to examine how fluctuations in temperature influenced the Guge Kingdom over the last 2000 years. Our record reveals relatively warm temperatures during the Medieval Climate Anomaly, cooling of 2 °C to –2 °C during the Little Ice Age, warming into the 18th century, and stabilization after 1800 CE. The temperature variations coincided with a transition of dynasties in Western Tibet. Temperature sensitivity tests on barley distribution, the principal cultivated cereal on Tibet, suggest that a decline in temperature led to a decreased crop yield that may have factored into the disappearance of the Guge Kingdom.

Key words: Paleothermometer; 5- and 6-methyl brGDGTs; temperature calibration; China; lacustrine sediments; the Common Era

Plain language summary

Paleoclimate reconstructions from lake sediments can provide a wealth of information on past climate changes. The accuracy of these reconstructions depends on a modern "translation" between proxies and climate variables. Lacustrine branched glycerol dialkyl glycerol tetraethers (brGDGTs) are viewed as a promising tool for reconstructing air temperatures. However, there is not a one-to-one correlation between air temperatures and lacustrine brGDGT-based temperatures, therefore we have to conduct calibration studies to understand how they are related. In this paper, we compared sediment traps in a meromictic and dimictic lake to determine niche partitioning of brGDGTs. Comparisons between core-top reconstructed and observed water column temperatures show that in meromictic lakes, brGDGTs are primarily produced in the lake bottom water, whereas in the dimictic lakes they are produced throughout the entire water column and reflect annual bottom water temperatures or water column temperatures during the mixing season. We then establish a new calibration and apply it to a lake sediment record, which indicates that temperatures cooled during 1630 CE. This time period coincides with the disappearance of the Guge Kingdom. Using ecological niche modelling, we confirm that cooling led to a decline in

barley, which has likely contributed to the collapse of Kingdom.

1. Introduction

The Tibetan Plateau (TP) and surrounding mountains contain the largest ice reservoir after the Arctic and Antarctic. This region is referred to as the Third Pole due to its cold temperatures at high elevations. Over the last century, temperatures at TP have warmed by up to 0.3 ºC per decade, which is three times faster than the global average (Qiu, 2008; Yao *et al.*, 2019). The increasing temperatures have resulted in 82% of the plateau's glaciers retreating during the last half-century (Yao *et al.*, 2019), and has led to a decline in the Tibetan crop yield (Tsechoe *et al.*, 2021). Paleoclimate reconstructions and historical records suggest that past civilizations from the Tibetan Plateau were also affected by climate change (Joshi *et al.*, 2021; Kathayat *et al.*, 2017), which likely influenced the availability of water resources (Li *et al.*, 2019; Xie *et al.*, 2021) and the growth of staple crops (Chen *et al.*, 2015). Existing terrestrial paleoclimate records from the TP, however, are limited due to a lack of empirical constraints on modern processes, low resolution and confounding factors such as precipitation, vegetation or lake water pH (Chen *et al.*, 2020; Liang *et al.*, 2019; Wang *et al.*, 2020b). This highlights the need for more robust, high-resolution temperature records in this area to improve our understanding of the magnitude of temperature change over the Common Era and the impacts of past climate change on human societies.

The Guge Kingdom was established in the end of the 10th century in the Western TP (Ngari region) and flourished for 700 years before collapsing c. 1630 CE (Joshi *et al.*, 2021; Kathayat *et al.*, 2017). Although several mechanisms have been proposed to explain the collapse of this lost Kingdom, including changes in crop patterns due to reduced monsoon rainfall (Kathayat *et al.*, 2017) and military conflicts with Ladakh Kingdom based on historical records (Yuan, 2009), it is unclear if decreasing temperatures also led to diminishing crop yields and contributed to the decline of the Kingdom. The staple grain of Ngari is Qingke barley, which is commonly grown in high altitude regions (4000 m a.s.l.). An aerial survey of abandoned agricultural fields from Bedongpo valley in the ancient Kingdom of Guge found that the area of historically cultivated fields was four times larger than the area cultivated today (Ryavec, 2015). Recent research has found that higher temperatures significantly decreased Tibetan barley production during the past three decades (Tsechoe *et al.*, 2021). Therefore, high-resolution climate records are needed to determine if changes in temperature led to a decline in barley production and contributed to the fall of the Guge Kingdom.

Branched glycerol dialkyl glycerol tetraethers (brGDGTs) are a promising proxy for paleotemperature as they are ubiquitous in soils (Naafs *et al.*, 2017a; Peterse *et al.*, 2012), peats (Naafs *et al.*, 2017b), marine sediments (De Jonge *et al.*, 2016; Dong *et al.*, 2015) and lake sediments (Feng *et al.*, 2019; Martínez-Sosa *et al.*, 2021; Russell *et al.*, 2018; Zhao *et al.*, 2022). BrGDGTs consist of glycerol moieties that are ether-bonded to *n*-alkyl side chains with varying methyl-additions (where a methylation at position α and/or ω5 are referred to as 5-methyl isomers, and α and/or ω6 are referred to as 6-methyl isomers) and up to two cyclopentane moieties (De Jonge *et al.*, 2013; Sinninghe Damsté *et al.*, 2000; Weijers *et al.*, 2006). BrGDGTs were initially developed as a temperature proxy by analyzing samples using high-performance liquid chromatography–mass spectrometry (HPLC-MS) with chromatographic separation on a Prevail Cyano column (Weijers *et al.*, 2007; hereafter termed "old method"). Empirical studies using this method found that the degree of Methylation of Branched Tetraethers (MBT) correlates with mean annual air temperature (MAAT), whereas variations in the degree of cyclization of brGDGTs, expressed as the Cyclization of Branched Tetraethers (CBT) index, correlates with soil pH (Peterse *et al.*, 2012; Weijers *et al.*, 2007). Improved chromatographic techniques allowed for the separation and quantification of 5- and 6-methyl brGDGTs (De Jonge *et al.*, 2014; Hopmans *et al.*, 2016; hearafter termed "new method"), a hybrid 5/ 6-methyl isomer (Weber *et al.*, 2015) and H-shaped brGDGTs (Baxter *et al.*, 2019; Naafs *et al.*, 2018; Tang *et al.*, 2021). Despite these improvements, brGDGT calibrations based on soil samples often overestimate regional MAAT when applied to sedimentary records, particularly in cold regions (MAAT < 5 °C) where brGDGT production likely occurs primarily during the warm season (Dang *et al.*, 2018; Zhang *et al.*, 2022; Zhao *et al.*, 2021). To constrain the primary source of brGDGTs in lakes, numerous studies have analyzed brGDGT distributions in suspended particulate matter (SPM), settling particles, surface sediments and catchment soils (Hu *et al.*, 2016; Loomis *et al.*, 2014; Miller *et al.*, 2018; Van Bree *et al.*, 2020; Weber *et al.*, 2018). These studies found that the production of brGDGTs depends on the extent and timing of lake mixing *vs*. stratification. However, this remains to be tested on a wider distribution of lakes across a range of lake mixing types.

In this study, we analyze 29 surface sediment samples from lakes in China alongside 39 additional surface sediment samples from a previously published dataset on Chinese lakes (Dang *et al.*, 2018). We produce a new brGDGT-temperature calibration. We apply the new calibration to our surface sediments and settling particles from sediment traps from two lakes with different mixing regimes (a dimictic lake and meromictic lake) to assess the validity of the calibration and identify a potential temperature bias related to seasonality and lake mixing. Moreover, we apply the new calibration to a published 2000-yr sediment core from Xiada Co (Li *et al.*, 2019), Western TP, to investigate the effect of MAAT changes on the Guge Kingdom. As we do not know the mixing types of Xiada Co, a lake energy balance model was applied to examine lake mixing events. We then combine the effect of MAAT with ecological niche modelling, based on the MaxEnt procedure, to improve our understanding of the impacts of climate change on a major food staple (Qingke barley) in Tibet. Using this approach, we aim to test whether climate change, mainly temperature, was responsible for changes in crop patterns in the Guge Kingdom during this time.

2. Methods

2.1 Field sampling and study sites

We collected surface sediments from 29 lakes on the Tibetan Plateau (TP) where there are numerous alpine lakes with limited human activities (Fig. 1; Table 1). Because there are few weather stations on the TP, MAAT at each site was obtained from the Worldclim2 dataset (Fick and Hijmans, 2017). The Worldclim2 database interpolates monthly temperature data compiled from globally distributed weather stations to 30 arc-seconds spatial resolution across a temporal range from 1970 – 2000 (Fick and Hijmans, 2017). We validate the Worldclim2 temperatures in TP through comparisons with MAAT from weather stations (Shiquanhe, Gaize, Lazi, Bange and Shenzha stations, from 1970 – 2000 and available from China Meteorological Data Service Centre). The temperature offset between the Worldclim2 MAAT and station MAAT from the TP ranges from -2.65 to 1.95 °C, suggesting that the Worldclim2 database can be used on TP. In the summer of 2013, we collected lake surface sediment samples and deployed 4 sediment traps at different depths (depths at 5, 15, 25 and 35 m) in the Dagze Co (31°54´ N, 87°33´E, central TP; Fig.1c) water column to collect settling particles deposited throughout the year. The following year, we collected the sediment trap samples and three surface sediment samples using an Ekman-

Birge grab sampler to compare the trap and surface sediment samples. All the samples were immediately placed in Whirl-Pak bags and stored at -20 °C in a freezer. We also deployed seventeen water temperature loggers (HOBO Water Temperature Pro v2 Data Logger) to continuously monitor temperature variability within the water columns of Dagze Co (depths at 5, 6, 7, 8, 9, 10, 11, 13, 15, 17, 19, 21, 23, 26, 29, 32 and 35 m) from August 2012 to July 2015 (Wang *et al.*, 2021a). Dagze Co is a brackish lake with a salinity of ~14.69 g/L at the surface that increases to 21.41 g/L at the bottom. The maximum water depth is 38 m and a permanent thermocline is present at 16–23 m (Wang *et al.*, 2014). We compared brGDGT distributions from the sediment traps and surface sediments from Dagze Co to previously published data from Lake 578 in southern Greenland (61°5´ N, 45°37´W; Fig. 1a), which is a dimictic lake and mixing occurs during spring and autumn (Zhao *et al.*, 2021). Lake 578 is a freshwater lake with a maximum depth of about 16 m. Sediment traps were set at 5 m, 10 m and 14 m depth and water temperature loggers were also deployed to monitor the water temperature changes from the summer of 2016 to 2019 (Zhao *et al.*, 2021). Each summer (2017, 2018, and 2019) the sediments traps were recovered. We use Lake 578 because its physical and chemical characteristics are similar to our TP lakes and has fully monitored records.

We apply our new calibration to a 2000 year-long lake sediment core from Xiada Co (33°23´ N, 79°21´; Li *et al.*, 2019). The core was collected in 2014 using a UWITEC piston corer from a depth of 19 m. Xiada Co is near the area of the Guge Kingdom, which could help us improve our understanding of the interactions between human and environmental changes (Fig. 1c). Xiada Co (XDC) is a freshwater lake (salinity ~0.15 g/L), fed by a river as well as glacial meltwater with a maximum depth of 20 m (Li *et al.*, 2019). The general characteristics of XDC are similar to Lake

578: both are small and alkaline (pH is ~9) lakes, with a similar lake depth (20 m and 16 m, respectively), freshwater (both <0.5 ppt), and MAAT of ~0 °C.

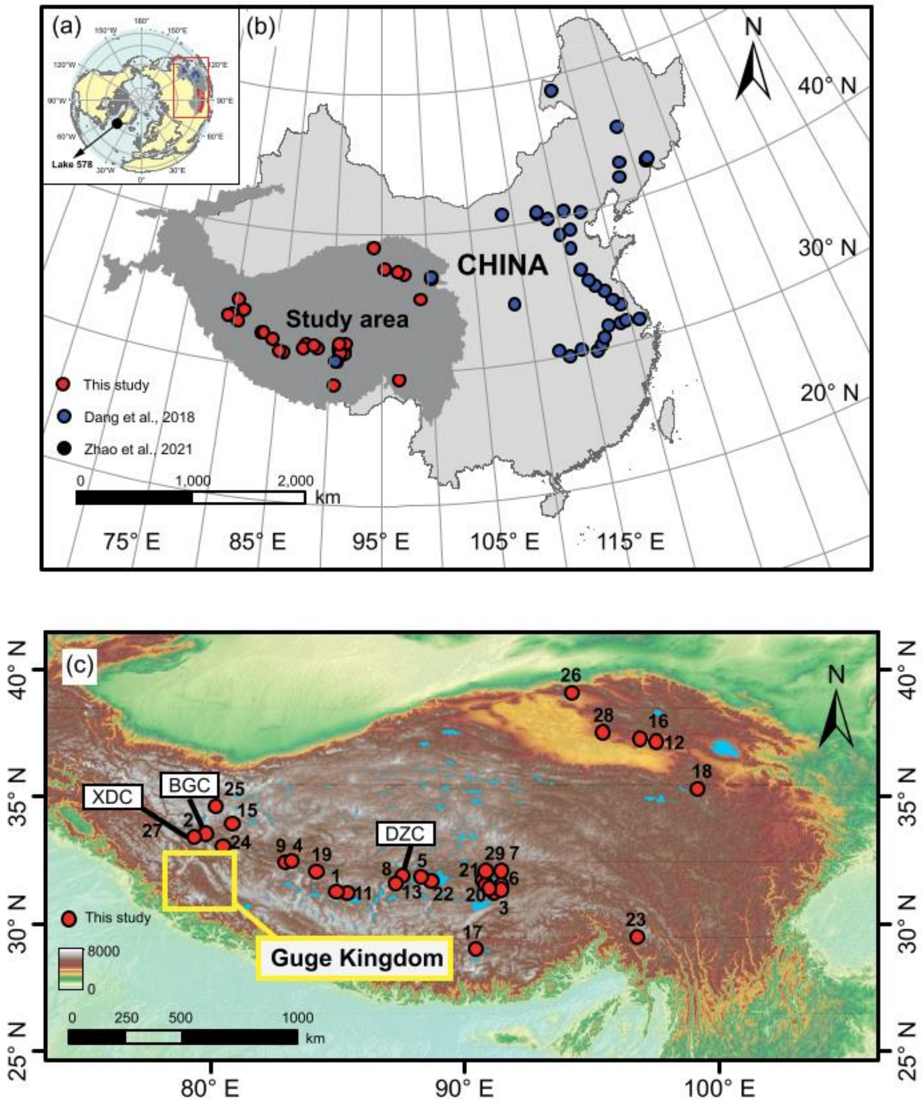

Figure 1. (a) Map of lake trap and surface sediment samples studied in this paper. (b) Map of China with the location of previously published Chinese surface samples (Dang et al., 2018) and new sites in this study, (c) focusing on the samples collected from the Tibetan Plateau for this study. The lakes labeled in the figure are as follows: 1. Anggu Co; 2. Bangong Co (BGC); 3. Beng Co; 4. Bieruoze Co; 5. Cuo Er; 6. Cuo Er2; 7. Cuo Na; 8. Darebu Co; 9. Daru Co; 10. Dawa Co; 11. Dagze Co (DZC); 12. Gai Hai; 13. Gemang Co; 14. Jiang Co; 15. Jieze Chaka; 16. Lake Keluke; 17. Kongmu Co; 18. Ku Hai; 19. Laguo Co; 20. Nairiping Co; 21. Peng Co; 22. Qiagui Co; 23. Lake Ranwu; 24. Rebang Co; 25. Songmuxi Co; 26. Lake Sugan; 27. Xiada Co (XDC); 28. Xiaochaidan; 29. Zigetang Co. The area of the former Guge Kingdom is the yellow rectangle.

2.2 GDGTs analysis and calibrations

About ~5–6 g of freeze-dried sediments were extracted by ultrasonic extraction with dichloromethane (DCM) : methanol (MeOH) (9 : 1, v/v; 3 times at 15 min; 30 °C). The total lipid extract was separated over a Al_2O_3 column using hexane : DCM (9:1, v/v) and DCM : MeOH (1 : 1, v/v) as eluents to isolate the non-polar and polar fractions (containing GDGTs), respectively. The polar fraction was dried under nitrogen gas, and dissolved in hexane : isopropanol (99 : 1, v/v) and then passed through a 0.45 μm PTFE filter prior to GDGT analysis.

Polar fraction analysis was performed using high performance liquid chromatography mass spectrometry (HPLC-MS). BrGDGTs were separated over three silica columns in tandem (Hypersil GOLD Silica, 100 mm× 2.1 mm, 1.9 μm) with a flow rate of 0.2 mL/min. For each sample, 10 µL were injected. The mobile phase consisted of 84% hexane and 16% ethyl acetate. The eluent procedure followed the method by Yang *et al.* (2015). This method allows for the separation of 5- and 6- methyl brGDGTs. Analyses were performed using selective ion monitoring (SIM) mode to track *m/z* 1050, 1048, 1046, 1036, 1034, 1032, 1022, 1020, and 1018. Peaks were identified manually based on previously published samples from East Africa (Russell *et al.*, 2018) and peak areas were integrated manually.

The fractional abundance, $f(x_i)$, for each brGDGT compound was calculated as follows and includes both the 5- and 6-methyl isomers:

$$f(x_i) = x_i/(\mathrm{Ia} + \mathrm{Ib} + \mathrm{Ic} + \mathrm{IIa} + \mathrm{IIb} + \mathrm{IIc} + \mathrm{IIIa} + \mathrm{IIIb} + \mathrm{IIIc} + \mathrm{IIa}' + \mathrm{IIb}' + \mathrm{IIc}' + \mathrm{IIIa}' + \mathrm{IIIb}' + \mathrm{IIIc}') \quad (1)$$

where x_i is any given brGDGT compound. Weijers *et al.* (2007) defined the methylation index MBT to estimate mean annual air temperature in global soil. De Jonge *et al.* (2014) subsequently redefined this index $\mathrm{MBT'}_{5\mathrm{Me}}$ based on new method using only 5-methyl isomers as:

$$\mathrm{MBT'}_{5\mathrm{Me}} = \frac{Ia + Ib + Ic}{Ia + Ib + Ic + IIa + IIb + IIc + IIIa} \quad (2)$$

Dang *et al.* (2016) found that the 6-methyl brGDGTs are correlated to temperature in Chinese lakes and defined the $\mathrm{MBT'}_{6\mathrm{Me}}$ index as:

$$\mathrm{MBT'}_{6\mathrm{Me}} = \frac{Ia + Ib + Ic}{Ia + Ib + Ic + IIa' + IIb' + IIc' + IIIa'} \quad (3)$$

We calculated the degrees of methylation of 5- and 6-methyl brGDGTs ($\mathrm{MBT'}_{5\mathrm{Me}}$ and $\mathrm{MBT'}_{6\mathrm{Me}}$) from our new samples combined with previously published Chinese surface sediment samples (Dang *et al.*, 2018; Table S1) and regressed with measured temperatures to develop a new brGDGT-temperature calibration (Figs. 3a – 3f). We compare applications using our new temperature calibrations with those from previously published calibrations from global lakes (Raberg *et al.* (2021); Martínez-Sosa *et al.* (2021), and regional lake calibrations (Dang *et al.*, 2018[China]; Dugerdil *et al.*, 2021 [Mongolian and Baikal]; Feng *et al.*, 2019 [Southwestern China]; Harning *et al.*, 2020 [Iceland]; Russell *et al.*, 2018 [East African]; Stefanescu *et al.*, 2021 [North America]; Zhao *et al.*, 2021 [South Greenland]) to evaluate the performance of our calibration (Figs. 3g &3h).

_ENREF_1

2.3 Statistical methods

To determine the largest modes of variance in our brGDGT dataset and assess the relationship between brGDGT fractional abundance and environmental variables (i.e., mean annual air temperature (MAAT), mean temperature of months above freezing (MAF T), summer air temperature (Summer T), lake depth, and pH), we performed a principal component analysis (PCA; Fig. S1a) and redundancy analysis (RDA; Fig. S1b), respectively. Dang *et al.* (2018) found different behaviors of brGDGT distributions between lakes from cold regions (MAAT < 5 °C) and warm regions (MAAT > 5 °C). Thus, we cluster brGDGTs from our expanded Chinese surface sediment dataset with MAAT below 5 °C and MAAT above 5 °C to distinguish brGDGT distributions for different temperature ranges (Fig. S1). To develop new calibrations, we calculated linear regressions of MBT'_{5Me} and MBT'_{6Me} in our surface sediment dataset and previously published Chinese surface sediment dataset (Dang *et al.*, 2018) with MAAT, MAF T and Summer T (Figs. 3a–3f). The correlation parameter R^2 and root mean squared error (RMSE) were calculated by bootstrapping 1000 times. All statistical analyses were performed using R (R Core Team, 2021; version 4.0.5) and the statistical software caret and vegan package (Kuhn, 2021; Oksanen *et al.*, 2020). We calculated the temperature bias (reconstructed temperature – observed temperature) for core-top sediments, settling particles from lake traps (Fig. 3g), and our new sites (Fig. 3h) using our calibration and previously published calibrations mentioned above.

A statistical regression approach in Fortran, RAMPFIT (Mudelsee, 2000), was employed to analyze our reconstructed temperature at Xiada Co to detect climate transitions. The data were detrended using a weighted least-squares method (WLS) to estimate the trend, which has previously been successfully applied to geochemical proxy time series (Li *et al.*, 2021a; Zhang *et al.*, 2021).

2.4 Lake model simulation

We investigated lake mixing events in Xiada Co by using a lake energy balance model (Dee *et al.*, 2018; Hostetler and Bartlein, 1990; Longo *et al.*, 2020). Due to a lack of sufficient observational datasets from Xiada Co, we adjusted the initial parameterizations of the lake model using parameterizations from lakes with similar characteristics (Table S2). The shortwave extinction coefficient was calculated by Secchi depth (Hutter *et al.*, 2014). A regional Chinese surface meteorological dataset was used to determine the inputs for near-surface air temperature and specific humidity values at 2 m above the land surface, wind speed at a height of 10 m, surface pressure, precipitation, and the downward shortwave and longwave radiation for 1979 – 2015 with a spatial resolution of 0.1×0.1° and a temporal resolution of 3 h (Chen *et al.*, 2011). An initial control simulation was run for 10 years. Due to the lack of direct observational data from Xiada Co, we validated the lake model results by comparing them to meteorological data from the Ngari Station For Desert Environment Observation and Research (2010 – 2015; Fig. S2a) and an observed temperature profile from a nearby lake (Bangong Co; 2013 – 2014; Table S3; Figs. 1c & S2b). Bangong Co is also a freshwater and dimictic lake (~0.47g/L salinity) with a maximum water depth of 42.6 m (Wang *et al.*, 2021a).

2.5 Qingke barley distribution

We employed species distribution modelling (SDM) to predict the distribution of Qingke barley (*Hordeum vulgare* L.) across space and time. There are various statistical methods and software implementations to use for SDMs, and among them, MaxEnt is widely applied for describing patterns and performing predictions even with incomplete datasets (Merow *et al.*, 2013).

There are two types of basic data for SDMs: species occurrence data and environmental variables. In this study, 77.35% of the species occurrence data was obtained through published field work (Zeng *et al.*, 2018) and the remainder of the data were sourced from the Global Biodiversity Information Facility (GBIF.org, 2019; GBIF). We selected only the data with precise location information and kept only one record in each evaluation unit (grid). Data from the literature was selected preferentially over GBIF data, and together we obtained 181 occurrence records for the model analyses. In order to distinguish the direct effect of temperature change on the distribution of Qingke barley, we chose two climatic variables, MAAT and annual precipitation (AP) from WorldClim2 database (Fick and Hijmans, 2017). With the current MAAT as a baseline, we generated two climate change scenarios, ne with a MAAT increase of 2 °C and the other with a MAAT decrease of 2 °C, and we assume that precipitation is constant in all scenarios.

We used the MaxEnt software platform (Phillips *et al.*, 2017) to project the distribution of Qingke barley. For the modeling process, 10-fold cross-validation was used to reduce uncertainty and generate an average probability of a suitable climate habitat map, the area under the extrinsic receiver operating characteristic (ROC) curve (AUC) values were used to assess the prediction accuracy, and ranged from 0.5 (random) to 1.0 (perfect discrimination). Further, we used a jackknife test to determine the relative importance of climatic variables. To further elucidate the environmental characteristics of suitable habitats, we built different MaxEnt models using single environmental variables (MAAT and precipitation) and then obtained response curves (Merow *et al.*, 2013; Yuan *et al.*, 2015), which determined how the logistic prediction changed with variations in each environmental variable.

3. Results

3.1 BrGDGT distributions in surface sediments, sediment traps and a downcore sediment record

The 5- and 6- methyl brGDGTs in all samples were chromatographically separated. Noncyclopentane moieties were predominant in our surface sediments samples (Fig. 2a). Across the 29 samples, the most abundant brGDGTs are pentamethylated brGDGTs (44%) followed by hexamethylated (39%) and tetramethylated (17%) brGDGTs (Fig. 2a). The new samples also contain higher fractional abundances of 6-methyl isomers, consistent with the previous published Chinese lake dataset (Dang *et al.*, 2018; Fig. 2a). However, the new samples differ from global lake brGDGT distributions, where pentamethylated brGDGTs (42%) are the most abundant followed by tetramethylated (31%) and hexamethylated (27%) compounds (Fig. 2a). The fractional abundance of brGDGTs in our dataset also contrasts with Chinese soils where pentamethylated brGDGTs constitute the largest fraction (47%) followed by tetramethylated (34%) and hexamethylated (18%) brGDGTs (Fig. 2b).

BrGDGT distributions in the settling particles from traps of Dagze Co and Lake 578 are consistent with our expanded surface sediment samples (Fig. 2c). In the Xiada Co down-core samples, brGDGTs are dominated by pentamethylated brGDGTs (42%) and hexamethylated (41%) brGDGTs (Fig. 2c), which is close to the brGDGT distributions found in surface sediments of the TP lakes analyzed in this study (Fig. 2c).

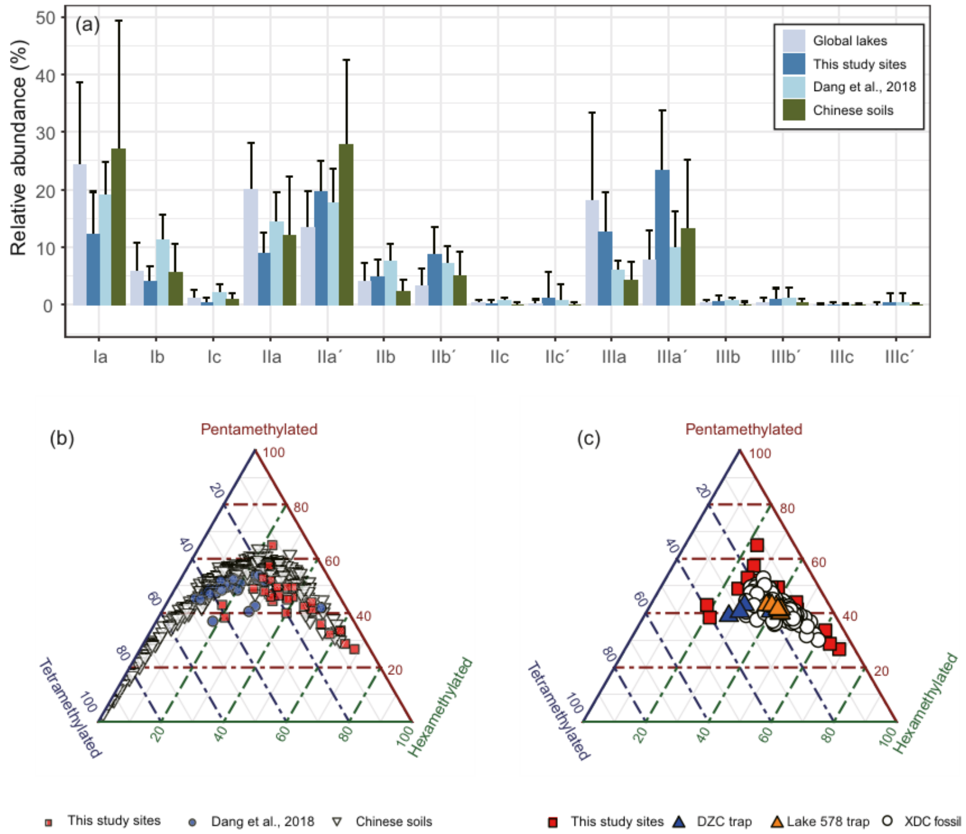

Figure 2. (a) Relative abundances of 5-methyl and 6-methyl branched tetraethers relative to total brGDGTs in global lakes compiled by Martínez-Sosa et al. (2021) with Raberg et al. (2021), and Chinese soils compiled by Crampton-Flood et al. (2020) with Duan et al. (2020) and Wang, An, et al. (2020), and lakes in China according to Dang et al. (2018) and this study. (b) Ternary plot of the abundance of tetramethylated, pentamethylated, and hexamethylated brGDGTs in the new sites, previously published Chinese surface sediment data set (Dang et al., 2018), and Chinese soils; (c) comparison of new surface sediment samples with Xiada Co down-core sediments (Li et al., 2019), Dagze Co (this study) and Lake 578 (Zhao et al., 2021) settling particles from the lake sediment traps.

3.2 Effects of environmental variables on brGDGTs and a new temperature calibration

The PCA of the brGDGTs did not show clear differences between brGDGT compounds from cold and warm regions (Fig. S1a). However, RDA reveals that the abundances of most 6-methyl brGDGTs are negatively related to temperature including MAAT, MAF and summer temperature, and tetramethylated brGDGTs are positively correlated with these temperature variables (Fig. S1b). To develop new calibrations, we compared the relationship of MBT'_{5Me} and MBT'_{6Me} with temperature in our expanded surface sediment dataset from Chinese lakes. Of the brGDGT indices that we tested, all temperature variables had a greater linear relationship with MBT´$_{6Me}$ than MBT´$_{5Me}$ (Figs. 3a – 3f). In addition, we find more 6-methyl brGDGTs in our studied lake sediments than 5-methyl brGDGTs (Fig. 2a) and Dang *et al.* (2018) also found that 6-methyl brGDGTs are correlated with temperature in Chinese lakes. Therefore, we developed the following new brGDGT-derived calibrations to mean annual air temperature (MAAT), summer temperature (Summer T) and mean temperature of months above freezing (MAF T) based on MBT´$_{6Me}$:

$$\text{MAAT} = 30.47 \times \text{MBT}'_{6Me} - 5.92 \qquad (R^2 = 0.63, \text{RMSE} = 4.04) \qquad (4)$$

$$\text{Summer T} = 18.72 \times \text{MBT}'_{6Me} + 4.39 \qquad (R^2 = 0.66, \text{RMSE} = 4.42) \qquad (5)$$

$$\text{MAF T} = 34.96 \times \text{MBT}'_{6Me} + 4.12 \qquad (R^2 = 0.60, \text{RMSE} = 2.66) \qquad (6)$$

3.3 Application of regional brGDGT calibrations to lake sediment traps, surface sediments and a core

We calculated the MAAT, Summer T and MAF T bias of settling particles from traps (Dagze Co and Lake 578) to evaluate the performance of our calibrations (Fig. 3g). Estimated biases of temperatures in Dagze Co and Lake 578 settling particles from traps revealed that bias ranges from -3.97 to 12.65 °C based on global lake calibrations (Martínez-Sosa *et al.*, 2021; Raberg *et al.*, 2021), from -34.02 to 27.86 °C based on site-specific calibrations (Feng *et al.*, 2019; Harning *et al.*, 2020; Zhao *et al.*, 2021), and from -12.56 to 32.81 °C based on regional calibrations (Dang *et al.*, 2018; Dugerdil *et al.*, 2021; Russell *et al.*, 2018; Stefanescu *et al.*, 2021). Our new MBT´$_{6Me}$-MAAT calibrations reconstruct temperatures for the sediment trap samples that are similar to annual temperatures recorded in the water column of Dagze Co, except at the chemocline (25m) where reconstructed temperatures are warmer than observed temperatures (Figs. 3g & 4d). In addition, the temperatures reconstructed from the settling particles by our new calibration did not reveal a summer or ice-free bias in Lake 578; rather, reconstructed temperatures reflect annual or mixing season water column temperatures (Figs. 3g &4e).

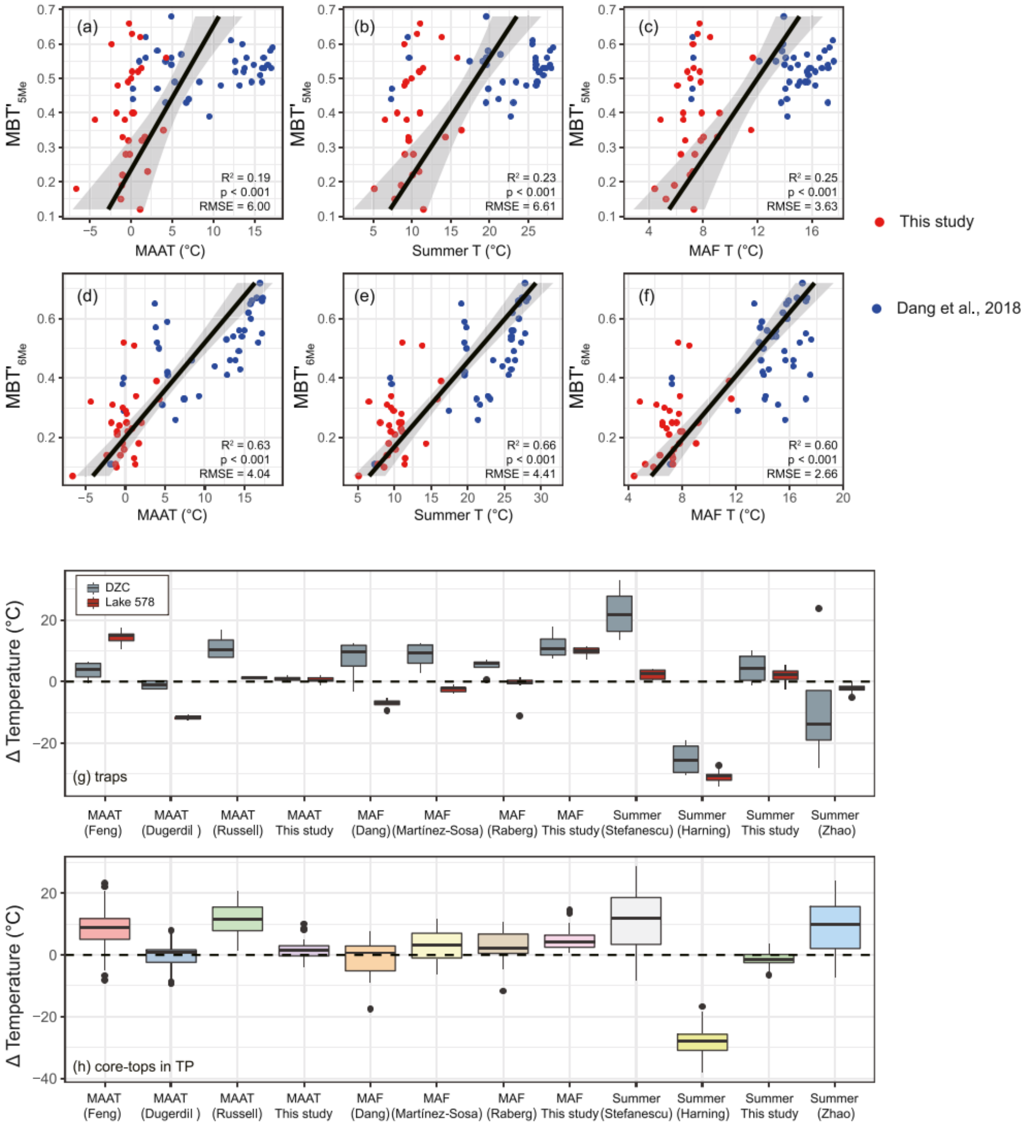

Figure 3. The relationship between brGDGT ratios and temperature, and bias comparison of new brGDGT-based calibration with previously published calibrations (Dang et al., 2018; Dugerdil et al., 2021; Feng et al., 2019; Harning et al., 2020; Martínez-Sosa et al., 2021; Raberg et al., 2021; Russell et al., 2018; Stefanescu et al., 2021; Zhao et al., 2021). (a–c) The relationship between MBT′5Me and MAAT, summer and MAF temperatures based on the study sites and previously published sites in China according to (Dang et al., 2018); (d–f) the relationship between MBT′6Me and MAAT, summer and MAF temperatures based on the Chinese lake data set; (g) boxplot summaries bias of different calibrations on settling particles from sediment traps in Dagze Co and Lake 578; (h) boxplot summaries bias of different calibrations on this study 29 new sites.

To evaluate the performance of new calibrations and published calibrations, we calculated the temperature bias of our 29 Tibetan surface sediment brGDGT-derived temperatures, i.e. the offset between reconstructed temperatures and observed temperatures (for example: for the MAAT calibration, we subtract the reconstructed MAAT from the observed MAAT). A boxplot summarizes the bias of different calibrations in our Tibetan surface sediment dataset (Fig. 3h). The estimated bias of the brGDGT-derived temperatures for our Tibetan lakes ranges from -11.66 to 11.64 °C for the global lake calibrations and from -17.43 to 28.65 °C for regional lake calibrations. The bias for a regional calibration from Mongolian lakes (-2.40 °C – 1.79 °C) and our new calibrations for MAAT (-0.56 °C to 3.04 °C) and summer temperature (-2.50°C to 0.33 °C) have a smaller temperature range than those from other calibrations and fall within the range of observed regional temperatures. Combined with lake trap results, we recommend our new MBT'_{6Me}-MAAT calibration for paleotemperature reconstructions in this region and similar regions.

To investigate whether lake mixing influences brGDGT-reconstructed temperatures from surface sediment, we applied our new calibrations Eq. 4, Eq. 5 and Eq. 6 to two different lake types: a meromictic lake, Dagze Co (Fig. 4a), and two dimictic lakes, Greenland Lake 578 (Fig. 4b) and Xiada Co (Fig. 4c). We observed different distributions of 5- and 6-methyl brGDGTs from surface sediments between the meromictic lake, Dagze Co, and the dimictic lakes, Lake 578 and Xiada Co (Fig. S3), despite they have similar MAAT. In the surface sediments from meromictic lake, Dagze Co, 6-methyl pentamethyl brGDGTs (IIa´, IIb´ and IIc´) were more abundant than in dimictic lakes (Lake 578 and Xiada Co; Fig. S3a). The reconstructed surface sediment temperatures based on MBT'_{6Me} -MAAT calibration are similar to annual lake bottom water temperatures in these three lakes, and are similar to lake column temperatures during the mixing season in the dimictic lakes (Lake 578 and Xiada Co; Table 2).

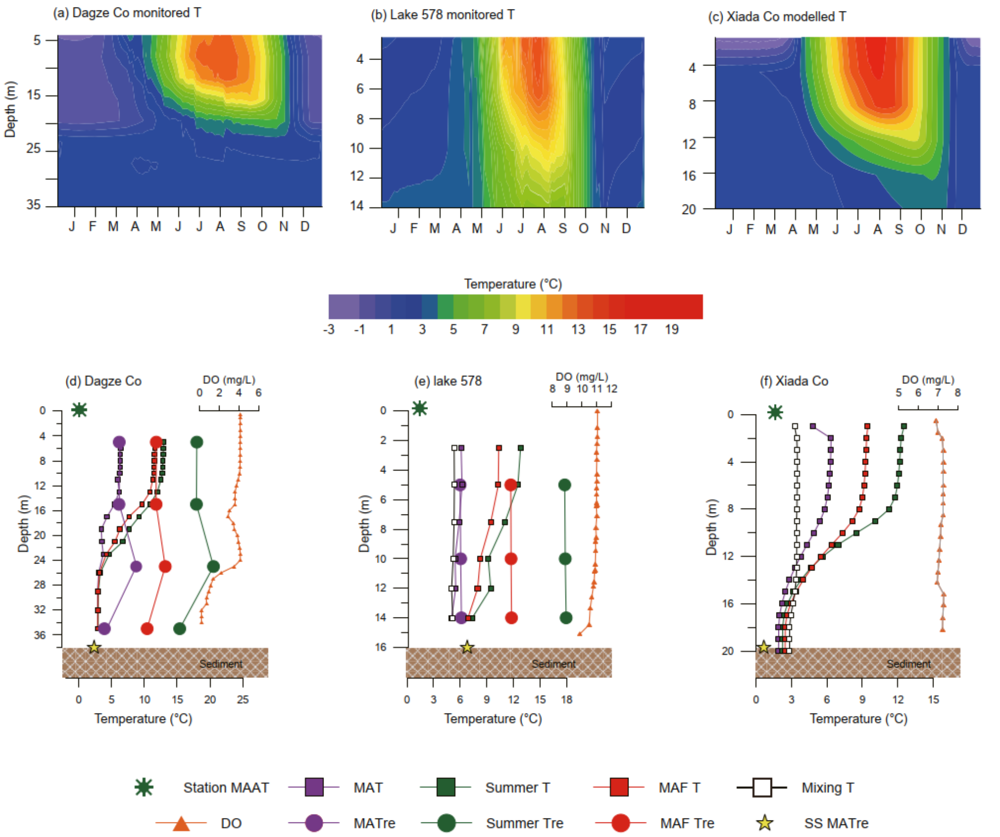

Figure 4. The lake water temperate profile indicating lake mixed types and reconstructed temperature based on this study calibration compared with observed water column temperature. Water temperate profile including (a) Dagze Co, (b) Lake 578, and (c) Xiada Co. Dagze Co data (average from 2012 to 2015; Wang et al., 2021), Lake 578 data (average from 2016 to 2019; Zhao et al., 2021), and Xiada Co data from a lake model (average from 1979 to 2015; this study). The Xiada Co temperature profile was generated using a lake-energy balance model (this study). Comparation of reconstructed temperature with monitored temperature at (d) Dagze Co, (e) Lake 578, and (f) Xiada Co. A dark green asterisk sign at the top of plots indicates the mean annual air temperature (MAAT) from station. The monitored water temperature plotted as squares for purple is mean annual temperature, green square is mean summer (June, July, and August) water temperatures, and red is mean water temperatures of month above freezing (MAF, range from May to October). The mixing events for Lake 578 (spring and autumn) and mixing season temperature are displayed as black-hollow squares. Temperature reconstructions based on our new calibrations are plotted as dots for settling particles from sediment traps deployed in the lake water column (purple dot using MBT′6Me-MAAT calibration Equation 4; green for MBT′6Me-Summer T calibration Equation 5 and red for MBT′6Me-MAF calibration Equation 6, and a yellow star refers to the temperature reconstruction from surface sediments based on MBT′6Me-MAAT calibration Equation 4.

For comparison, we also applied previously published global calibrations (Martínez-Sosa *et* al., 2021; Raberg et al., 2021) and our new MBT'_{6Me} -MAAT with MBT'_{6Me} -MAF calibrations to global lake surface sediments to different lake mixing types. In the stratified lakes, 6-methyl brGDGTs (IIa´, IIb´,IIc´ and IIIa´) were more abundant than 5-methyl brGDGTs (IIa, IIb, IIc and IIIa, Fig. S4), whereas 6-methyl brGDGTs (IIa´, IIb´, IIc´ and IIIa´) were less abundant than 5-methyl brGDGTs in the mixed lakes (IIa, IIb, IIc and IIIa, Fig. S4). The results show that our MBT'_{6Me} - MAAT calibration and Martínez-Sosa et al. (2021) calibration work well in mixed lakes (Fig. 5a), but our calibration underestimates temperatures (average -4.72 °C) in stratified lakes, particularly around the low latitudes (Fig. 5b).

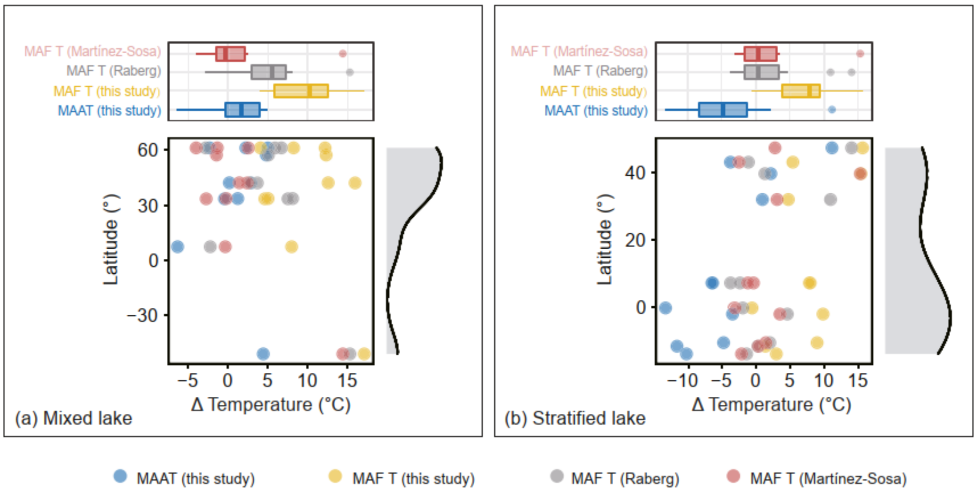

Figure 5. Comparison of the bias of brGDGT-derived temperatures with measured temperatures between (a) mixed lakes and (b) stratified lakes based on from ours MBT′6Me-MAAT and MBT′6Me-MAF calibration (Equations 4 and 6), and the global calibrations Martínez-Sosa et al. (2021) and Raberg et al. (2021). In (a) and (b), bottom left scatterplots show bias of different calibrations derived temperatures across different latitudes (compiled and revised from Martínez-Sosa et al., 2021), blue dot, MBT′6Me-MAAT calibration from this study; yellow dot, MBT′6Me-MAF calibration from this study; gray dot, calibration from Raberg et al. (2021); and red dot, calibration from Martínez-Sosa et al. (2021). Bottom right near the scatterplots represents the density of each site corresponding to the scatterplots. Top boxplot shows the median and the 5th, 25th,75th, and 95th of bias from each calibration corresponding to the scatterplots. The global calibrations and our MBT′6Me-MAF calibration were developed for MAF, the bias of these two calibrations was calculated by reconstructed temperature minus measured MAF. As our MBT′6Me-MAAT calibration is for MAAT, our bias was calculated by reconstructed temperature

minus measured MAAT. The mixed lakes include Flatworm Lake, Robe Lake, Lago de Sanabria, Laguna Amarga, Lago Grande Estana, Mother Goose Lake, Allison Lake, Bangong Co, Lake 578, and Xiada Co. Stratified lakes include Big Soda Lake, Lake Malawi (LS21), Lake Kivu, Lake Malawi (LS28), Deming Lake, Crater Lake, Lake Edward, Big Croc Lake, Lake Malawi (LS48), Hot Water Lake, and Dagze Co.

We reconstructed temperature variations recorded in a previously published Xiada Co sediment core (XDC) from Li *et al.* (2019) based on our new calibration (MBT'_{6Me} -MAAT calibration; Eq. 4) and compared our reconstructed MAAT with a meteorological dataset spanning the past 37 years (Figs. 6a & 6b). Our record follows the trend of the meteorological temperatures with a minimum around ~ 2000 CE and relatively high MAAT before and after 2000 CE (Fig. 6a). Furthermore, the top-most sample at XDC (0–1cm, ~2013 CE) was 1.70 °C, very close to the lake column water temperature during mixing season and the bottom water temperature (3.31 °C and 2.19 °C, respectively), but different from annual lake water temperatures (4.25 °C). The value of average bottom temperature or mixing season lake water column temperature are very close to the meteorological station MAAT (1.63 °C, Table 2). Thus, our brGDGT-based temperature reconstruction from XDC could reflect MAAT. Above all, these comparisons support the applicability of our new MBT'_{6Me} -MAAT calibration (Eq. 4) as a reliable MAAT calibration in Tibet.

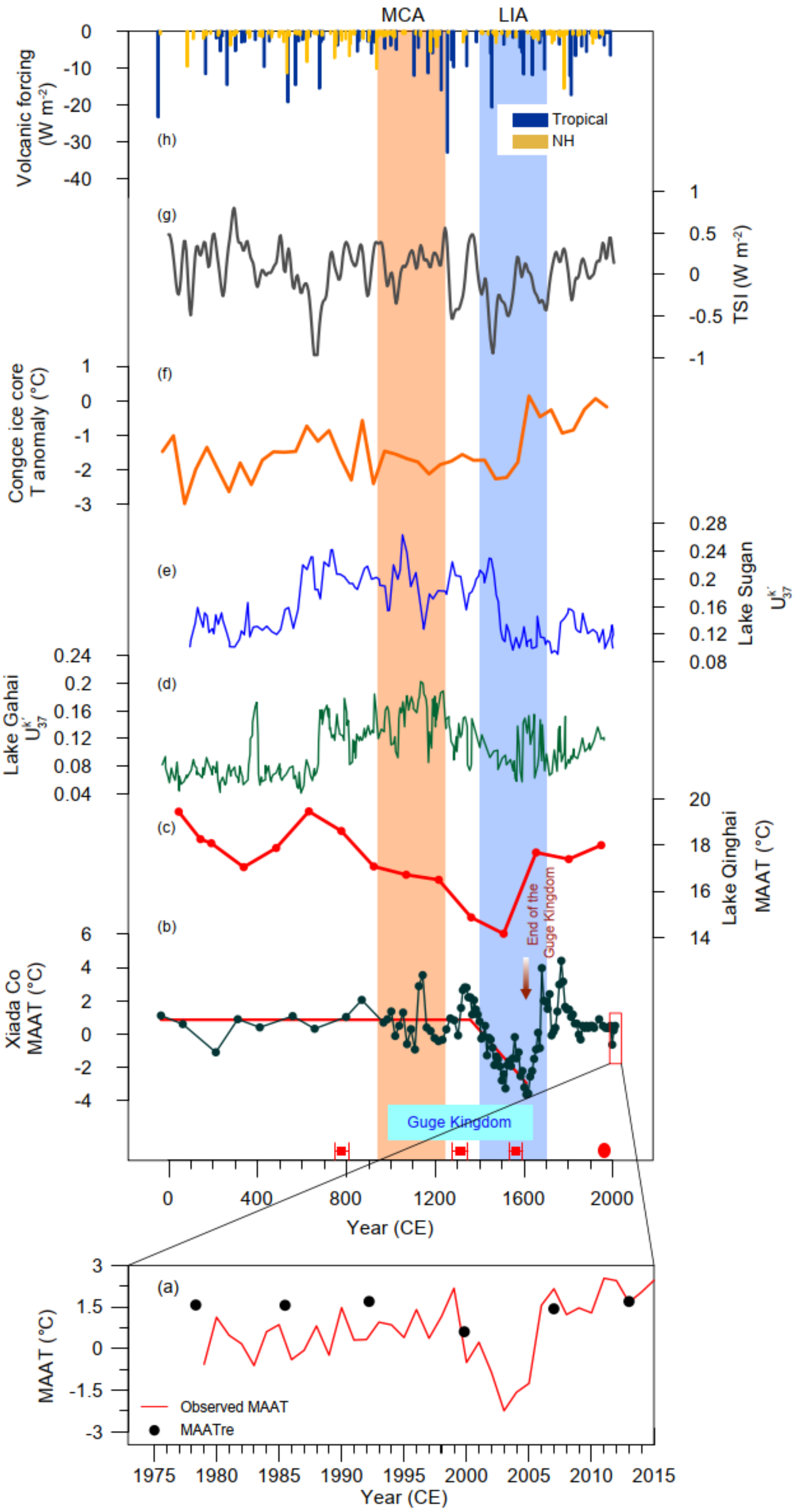

Figure 6. Major climate changes over the last 2000 years on Tibetan Plateau are shown (red box plots represent calibrated 14C ages and red dot is 210Pb and 137Cs age), including (a) the comparison of recent brGDGT reconstructed temperatures from Xiada Co (black line with plus sign) with ~37 year (1979–2015 CE) annual air temperature data (blue line) from Chen et al. (2011); (b) brGDGT reconstructed temperature during past 2000 years from Xiada Co (this study).

The red line indicates transitions in our reconstructed temperature identified by RAMPFIT (Mudelsee, 2000); (c) MAAT reconstruction based on alkenones from Lake Qinghai (in east-northern Tibet; Hou et al., 2016); temperature proxy (U_37^k') based on alkenones from (d) Lake Gahai and (e) Sugan respectively (both in east-northern Tibet; He et al., 2013); (f) temperature anomaly reconstruction based on ice cores δ18O from Chongce (in north-western Tibet; Pang et al., 2020); (g) changes in total solar irradiance (TSI; Schmidt et al., 2011) and (h) volcanic forcing from tropical and Northern Hemisphere eruptions (Sigl et al., 2015).

Our reconstructed MAAT at XDC fluctuates between –2.26 °C and 5.44 °C and the average MAAT is 1.45 °C. In the revised XDC temperature record we observe a similarly strong relationship with meteorological data (Fig. 6b), and a warmer (~1.84 °C) period between 900–1250 CE. A RAMPFIT analysis reveals that there is a sudden decrease in MAAT around 1400 CE, and a relatively cool (~0.11 °C) period from 1400 – 1700 CE, which coincides with the fall of the Guge Dynasty (Fig. 6b). The brGDGT reconstruct MAAT trends are consistent with alkenone-derived reconstructions (Figs. 6c – 6e) and ice core $\delta^{18}O$-inferred MAAT in Tibet (Fig. 6f). The record indicates cooling from 1400 – 1700 CE, consistent with lower insolation (Fig. 6g) and a high frequency volcanic eruption (Fig. 6h).

3.4 Qingke Barley simulation

MaxEnt provided an average test AUC for the replicate runs of 0.88 and a standard deviation of 0.03 indicating satisfactory model performance. The analysis demonstrates that MAAT is the primary determinant of barley distribution, with contribution rates of 63.4%, whereas precipitation is a secondary determinant with a contribution rate of 36.6%. The response curves reflect the dependence of predicted suitability both on the selected variable and on the dependencies induced by correlations between the selected variable and other variables (Fig. S5). We carried out temperature sensitivity tests for barley by changing temperatures (adding or subtracting 2 °C from modern temperatures) and keeping precipitation constant. The temperature sensitivity tests reveal that there are stark differences under different temperature simulations (Figs. 8a – 8c). The optimal range of MAAT for Qingke barley is 0 – 8 °C (Fig. 8d).

4. Discussion

4.1 Source of brGDGTs in surface sediments

The source of brGDGTs in lacustrine sediments should be carefully identified as there are two potential sources, including terrestrial input from catchment soil and *in situ* production in lake water column or surface sediments. Cao *et al.* (2020) found that some brGDGT-inferred indices were significantly different between catchment soil and lake suspended particulate matter (SPM) and implied that the production of brGDGTs in the lake itself in Gonghai, China. Van Bree *et al.* (2020), using 17-month site-specific conditions, found contrasting brGDGT distributions between soils and SPM from oxygenated and anoxic parts of the water column, suggesting that brGDGTs from Lake Chala, a crater lake on the border of Kenya and Tanzania, have an aquatic source. As these studies focus on individual lakes, they are able to distinguish between allochthonous inputs from soils and autochthonous production in the lake water column and/or surface sediments. We compared our datasets with published Chinese soil datasets (Ding *et al.*, 2015; Duan *et al.*, 2020; Lei *et al.*, 2016; Wang *et al.*, 2016; Wang *et al.*, 2020a; Xiao *et al.*, 2015) and global lake datasets compiled by Martínez-Sosa *et al.* (2021) and Raberg *et al.* (2021) to determine the likely brGDGT sources at our study sites.

Comparison between the fractional abundances of brGDGTs in Chinese soils, in global lakes, in a previous published Chinese lake dataset, and in our dataset reveals that the distributions of non-cyclic brGDGTs found in Chinese soils and lakes are similar to the non-cyclic brGDGT distributions found in the global lake dataset (Fig. 2a). However, the expanded Chinese lake dataset, which includes the new dataset developed in this study and a previous published dataset (Dang *et al.*, 2018), contain high fractional abundances of 6-methyl brGDGTs (IIb´, IIc´, IIIa´, IIIb´ and IIIc´), which contrast with the global lake and Chinese soil datasets. The high fraction of 6-methyl brGDGTs are likely derived from *in situ* lacustrine production (Dang *et al.*, 2018; Russell *et al.*, 2018), as 6-methyl brGDGTs prefer oxic aquatic environments (Wu *et al.*, 2021). The global lake dataset includes a large proportion of tropical lakes where oligomixis is common in contrast to northern temperate lakes, which have a large proportion of dimictic and polymictic lakes (Woolway and Merchant, 2019). Oligomictic and meromictic lakes are permanently stratified, and both generally possess an anoxic hypolimnion, whereas dimictic or polymictic lakes mix two or more times a year and bring oxygen from the surface water into the hypolimnion (Zadereev *et al.*, 2017). We posit that these different 5- and 6-methyl brGDGT distributions stem from lake mixing types and their impacts on dissolved O_2 (DO), as bacteria preferentially produce 6-methyl brGDGTs when thriving in oxic environments and 5-methyl brGDGT concentrations increase under anoxic conditions (Wu *et al.*, 2021). Our combined evidence indicates that the lakes in our study have an *in situ* source, while terrestrial input is negligible.

4.2 Environmental controls on brGDGT production in lakes

RDA analysis for abundances of brGDGTs and environmental variables in Chinese lakes indicate that tetramethylated and pentamethylated 5-methyl compounds positively correlate with MAAT, whereas IIIa, IIIa´ and pentamethylated 6-methyl compounds negatively relate to MAAT

(Fig. S1b). Similarly, previous studies also showed that tetramethylated brGDGTs are positively correlated to MAAT, whereas IIIa is negatively correlated with MAAT (De Jonge *et al.*, 2014; Russell *et al.*, 2018). However, Russell *et al.* (2018) found that IIIa´ and IIa´ are orthogonal to MAAT, suggesting IIIa´ is not correlated to MAAT. This contrasts with our data, in which the abundance of IIIa´ and IIa´ are negatively correlated to MAAT ($r = -0.7$, $p < 0.001$ and $r = -0.3$, $p < 0.02$ respectively).

Previous studies suggest that lake depth, seasonality, salinity and dissolved oxygen content were important variables controlling the brGDGT production in many (Dang *et al.*, 2018; Raberg *et al.*, 2021; Stefanescu *et al.*, 2021; Wu *et al.*, 2021) though not in all lake sediments (Russell *et al.*, 2018). To determine if lake depth influences brGDGT-derived temperatures, we selected three lakes with similar MAAT (~0.2 °C) and different lake depths: Dagze Co (0.31 °C, 38 m), Laguo Co (0.14 °C, 18 m) and Bieruoze Co (0.13 °C, 2 m). For each of these lakes, the reconstructed brGDGT temperatures using the MBT'_{6Me}-MAAT reconstructions are very close to the observed MAAT (Dagze Co, 0.31 °C; Laguo Co, 0.14 °C; Bieruoze Co, 0.12 °C), regardless of the lake depth. Our RDA results show that lake depth is positively correlated with 6-methyl (IIa´, IIb´, IIIa´, IIIb´ and IIIc´) and negatively correlated with pentamethyl (IIa, IIb and IIc) and tetramethyl (Ia, Ib and Ic) brGDGTs (Fig. S1b). The lake depth is orthogonal to IIIa, suggesting a weak relationship between IIIa and lake depth in our dataset (Fig. S1b). Our new MBT'_{6Me}-MAAT reconstructions was not influenced by differences in lake depth. In our calibration, the MBT'_{6Me} depends on tetramethylated and 6-methyl brGDGT production, which occurs primarily under oxic conditions (Weber *et al.*, 2018; Wu *et al.*, 2021) and therefore should be independent of lake-mixing type and lake depth. In contrast, previous calibrations relied on the 5-methyl brGDGTs which are also produced under anoxic conditions (Weber *et al.*, 2018; Wu *et al.*, 2021), and thus might be produced in higher abundance in the bottom water of seasonally stratified lakes during the summer months. As our new calibration includes tetramethylated and 6-methyl brGDGTs, it should be suitable for a wider-range of lake mixing-types and therefore provide a more reliable MAAT reconstruction without seasonal bias.

Quantitative lacustrine brGDGT calibrations for MAAT can yield estimates biased toward the warm season. Analyses from compiled global lake sediments also find that the mean temperature of months above freezing (MAF) have the highest relationship with brGDGT indices (Martínez-Sosa *et al.*, 2021; Raberg *et al.*, 2021). Cao *et al.* (2020) investigated suspended particulate matter (SPM) in Gonghai Lake, China and found that brGDGT-derived temperatures were similar to the mean annual lake water temperature. The decoupling between lake water temperature and air temperature in the winter can lead to a warm bias in brGDGT-reconstructed temperatures in mid- to high-latitude regions (Cao *et al.*, 2020). In our studied meromictic lake, Dagze Co, settling particles in the lake sediment trap are well correlated with mean annual temperature (MAT) rather than MAF temperature or summer temperature except at the chemocline (at 25 m) (Fig. 4d). The trap in the chemocline is located at the depth with the highest DO concentration which may result in changes in bacterial community composition. De Jonge *et al.* (2019) found that the bacterial community changes have a strong influence on the brGDGT-derived temperature. The brGDGT-derived temperature at Dagze Co surface sediment (2.36 °C) is closely related to the mean annual lake bottom water temperature (2.86 °C). In the dimictic lake, Lake 578, brGDGT-derived temperatures from settling particles also reflect MAT or mixing season lake water temperature rather than summer air temperatures or MAF temperatures (Fig. 4e). The brGDGT-derived temperature for the surface sediment samples from Lake 578 is 6.81 °C, which is similar to lake bottom water temperatures (5.04 °C) or mixing season lake water temperatures (5.24 °C). BrGDGTs from Lake Lucerne in central Switzerland were also biased towards winter temperatures due to water column mixing in the winter months (Blaga *et al.*, 2011), as were temperatures in a dimictic lake in the northeastern US (Loomis *et al.*, 2014). We propose that brGDGT-derived temperatures may relate to bottom water temperatures in meromictic lakes and mixing season or annual bottom lake water temperatures in dimictic lakes, producing a seasonal of depth-dependent bias in these lakes due to increased production of 6-methyl brGDGTs in the bottom water or during mixing.

DO concentration may be another important factor when reconstructing temperatures for lacustrine brGDGTs (Weber *et al.*, 2018; Wu *et al.*, 2021; Yao *et al.*, 2020). Loomis *et al.* (2014) found that in Lower King Pond in temperate northern Vermont, USA, the highest flux of brGDGTs occurred during periods of spring and fall isothermal mixing, similar to what we find in Lake 578, Greenland (Zhao *et al.*, 2021). This is in contrast to the low brGDGT flux in settling particles during the deep mixing season from tropical Lake Chala (a permanenently statified and deep (but partial) mixing lake; Van Bree *et al.*, 2020). We infer that changes in DO result from different mixing events in these lakes and therefore influence brGDGT production. Recent culture experiment indicates that O_2 availability controls biosynthesis of brGDGTs by *Edaphobacter aggregans*, an Acidobacteria (Halamka *et al.*, 2021). Our results are consistent with previous studies that brGDGT concentrations are significantly related to water column DO concentrations (Martínez-Sosa and Tierney, 2019; Weber *et al.*, 2018; Wu *et al.*, 2021; Yao *et al.*, 2020). Again, this emphasizes the importance of lake mixing types on brGDGT distributions, as we discussed above.

4.3 Assessment of the new brGDGT calibration

While there is substantial agreement for the relationship between brGDGT distributions and temperature, there is little understanding of how accurately the brGDGT-temperature relationship represents the transition between lake and air temperatures. Stefanescu *et al.* (2021) found that in both shallow and deep lake surface sediments from North America the MBT´$_{5Me}$ index is strongly correlated to lake bottom water temperatures. Similarly, brGDGTs in the Dagze Co surface sediment reflect lake bottom water temperatures (Table 2; 2.36 °C in surface sediment MBT´$_{6Me}$-MAAT; 0.17 °C in observed station MAAT, 2.86 °C in observed annual bottom water temperatures according to Wang *et al.* (2021a)). When we apply our new MBT´$_{6Me}$ -MAAT calibration developed from expanded Chinese lake surface sediments to Xiada Co, brGDGT reconstructed temperatures in the surface sediments (0.4 °C) and top-most sample (0–1 cm) from Xiada Co down-core sediments (1.7 °C) are close to annual bottom water temperatures (2.19 °C from lake model) and mixing season water column temperature (3.31 °C from lake model) (Table 2). This representing different lake water temperatures may be related to the different thermal regimes of these two lakes as Dagze Co is a meromictic lake (Wang *et al.*, 2021a), whereas Xiada Co is a dimictic lake based on our lake model (Fig. 4c). This phenomenon is also found in the site-specific study from Lake 578 (Zhao *et al.*, 2021), where both brGDGTs in settling particles and surface sediment were consistent with mean annual lake bottom temperatures or water temperatures during the mixing seasons (Fig. 4e and Table 2). The fractional abundance of 6-methyl brGDGTs in both surface sediments and sediment traps from meromictic lake Dagze Co are higher than dimictic Lake 578, which could be interpreted to the seasonality of brGDGT production. The flux of brGDGTs to surface sediment is highest during period of isothermal mixing in mixed lake (Loomis *et al.*, 2014), whereas year-round fluxes of brGDGTs come from bottom water in stratified lakes (Weber *et al.*, 2018). This was also found in surface sediments from globally stratified and mixed lakes, where 6-methyl brGDGTs (IIa´, IIb´,IIc´ and IIIa´) were more abundant than 5-methyl brGDGTs (IIa, IIb, IIc and IIIa) in stratified lakes and 5-methyl brGDGTs (IIa, IIb, IIc and IIIa) dominated in mixed lakes (Fig. S4). Another site-specific study from a dimictic lake, Huguangyan Maar Lake (in China), also revealed that brGDGT-reconstructed MAATs were similar to observed lake bottom temperatures and reconstructed temperatures were cooler than observed MAATs during lake thermal stratification (Hu *et al.*, 2016). The reconstructed MAATs based on brGDGTs from other meromictic lakes also reflects bottom water temperatures in Basin Pond (from USA; Miller *et al.*, 2018), Lugano (from Switzerland; Weber *et al.*, 2018) and Lake Chala (from Africa; Van Bree *et al.*, 2020). In general, the temperature reconstructed by brGDGT-producing heterotrophic bacteria in lake sediments are more similar to bottom water temperatures in meromictic lakes, and likely biased towards bottom water or mixing season water temperature in a mixed lake.

Numerous brGDGT-MAAT calibrations have been developed for local (Dang *et al.*, 2018; Dugerdil *et al.*, 2021; Russell *et al.*, 2018; Stefanescu *et al.*, 2021), site-specific (Feng *et al.*, 2019; Harning *et al.*, 2020; Zhao *et al.*, 2021) and global (Martínez-Sosa *et al.*, 2021; Raberg *et al.*, 2021) temperature reconstructions; however, in order to apply these calibrations to temperature reconstructions we also need to evaluate their accuracy at a given location. We tested previously published calibrations using our 29 core-tops from the Tibetan Plateau and settling particles from lake traps to investigate the accuracy of our new calibration. In calibrations from similar regions, brGDGT-based temperatures from Iceland, for instance, are strongly biased towards colder temperatures, while in Greenland the brGDGT-calibration is biased towards colder temperatures in trap samples and warmer temperatures in core-top samples (Fig. 3g and 3h). These calibrations, however, were based on one site, whereas ours cover a broader geographical area and diverse lake-types. The core-top samples and settling particles from traps in our new calibration (MBT'_{6Me}-MAAT; Eq. 4) accurately replicate observed MAAT, which suggests that the new calibration for MAAT is a robust way to investigate brGDGTs in Tibetan lacustrine sediments (Figs. 3g & 3h).

Previous analyses using brGDGTs did not consider the influence of lake mixing due to limited knowledge of lake mixing types. We find that lake mixing type has a strong influence on brGDGT-derived calibration. Our calibration performs better in mixed lakes (data from Martínez-Sosa *et al.*, 2021; Fig. 5a), which are typically located in mid- to high-latitude regions where mean annual lake bottom-water temperatures and mixing season temperatures more closely reflect mean annual air temperatures. However, our calibration does not work well in meromictic lakes because most of these lakes in which brGDGTs have been studied are located near the equator, where the bottom water temperature is on average cooler than MAAT (Katsev *et al.*, 2017; Lewis Jr, 1973). The reason for a warm bias might occur in meromictic lakes from mid- to high latitude regions is that lake bottom water temperatures are near 4 °C and could be warmer than the MAAT, such as observed in Dagze Co (Fig. 4d). Our study shows that lake mixing type is a significant factor that influences the production of 5- and 6-methyl brGDGTs in lakes, and in turn influences reconstructed temperatures. Dee *et al.* (2018) also found that mixing depth profoundly impact the relationships between lake temperature and air temperature in lake models, and we must therefore consider mixing depth, lake surface and bottom water temperatures when developing temperature reconstructions.

4.4 Potential relationship between temperature change and the fall of the Guge Kingdom

The reconstructed past temperature from Xiada Co (Western Tibet), which is located near the ruins of Guge Kingdom, could help us understand how past human civilizations responded to rapid environmental changes (Fig. 1c). As discussed above, the top-most MBT'_{6Me}-MAAT reconstruction in Xiada Co represent lake column temperatures during mixing season, which fall within the range of station observed air temperatures from 2010 to 2015. Our reconstruction provides an opportunity to test how internal climate variability and external forcing influenced temperature changes during the Common Era. General characteristics of our reconstructed temperature change are well-expressed by brGDGTs during the last two millennia, and agree well with other published Chinese composite temperature records (Ge *et al.*, 2013). According to our reconstructions and RAMPFIT analysis, MAAT was stable with an average value of 1.83 °C before 1300 CE and with one warm peak around 1150 CE. This warm period was also found in Lake Sugan and Gahai, located at Eastern TP (He *et al.*, 2013; Figs. 6d & 6e). Following this period, MAAT decreased from 4 °C to –2 °C during the 14^{th} to 17^{th} century, during which time previous reconstructions indicate that precipitation did not change (Figs. 7e & 7f). This time period corresponds to a total solar irradiance minima and frequent volcanic activity (Figs. 6g & 6h). Other proxy records in Tibet including brGDGTs, alkenones and ice core $\delta^{18}O$ also display clear cooler temperatures, about 2 °C, during this period than present (Fig. 6; He *et al.*, 2013; Hou *et al.*, 2016; Hou *et al.*, 2019; Li *et al.*, 2017). The slight temporal discrepancies can partly be explained by the various proxies used and the dating uncertainties. After the LIA, MAAT increased gradually through the 17th and 18th centuries, until it stayed at the average value of 1.67 °C during the last 200 years.

The core region of the Guge Kingdom was in arid canyon country in the watershed of the Xiangquan River. During the heyday of the Kingdom in the 11th century, Guge became a politically and economically important region. It flourished for 700 years yet dissolved in the 17th century (Ryavec, 2015). The reason for the fall of the Kingdom remains poorly understood. One possible reason for its demise is the aridity during the LIA (~1630 CE), as it occurred in concert with an Indian summer monsoon minimum (Kathayat *et al.*, 2017). However, it should be noted that Guge lies in an arid climate where monsoonal moisture is blocked by the high Himalayas, and even now the precipitation in the area is only ~90 mm/yr, meaning that precipitation may not be the only water source for local people. Our analysis indicates that the suitable temperature for Qingke barley range between 0 and 8 °C (Fig. 8d) and precipitation range between 300 – 800 mm is optimal for barley growth (Fig. S6). The precipitation is below 100 mm/year today in this area, and it has not changed significantly over the past 2000 years (Figs. 7e & 7f). Thus, we focus on the effect of temperature changes on agriculture.

We found temperature oscillations contributed to significant crop yields (Fig. 8). Our sensitivity niche modelling test of present-day Qingke barley distributions with temperature sensitivity test suggests decreasing temperature led to a loss of optimal habit in the southwest TP (Figs. 8 a–c). Tsechoe *et al.* (2021) found that crop yield sensitivity increased in response to temperatures rise under a warmer climate over the past three decades. In addition, the average chain length (ACL) of fatty acids, indicative of vegetation history in this region, showed increasing ACL values since the LIA, reflecting an arid environment and a decrease in vegetation (Fig. 7c). These results corroborates the finds of Wei *et al.* (2020) that a major reduction in barley during the LIA based on barley pollen records (Fig. 7b), suggest that a decline in temperature led to a decreased crop yield and may have contributed to the demise of the Guge Kingdom.

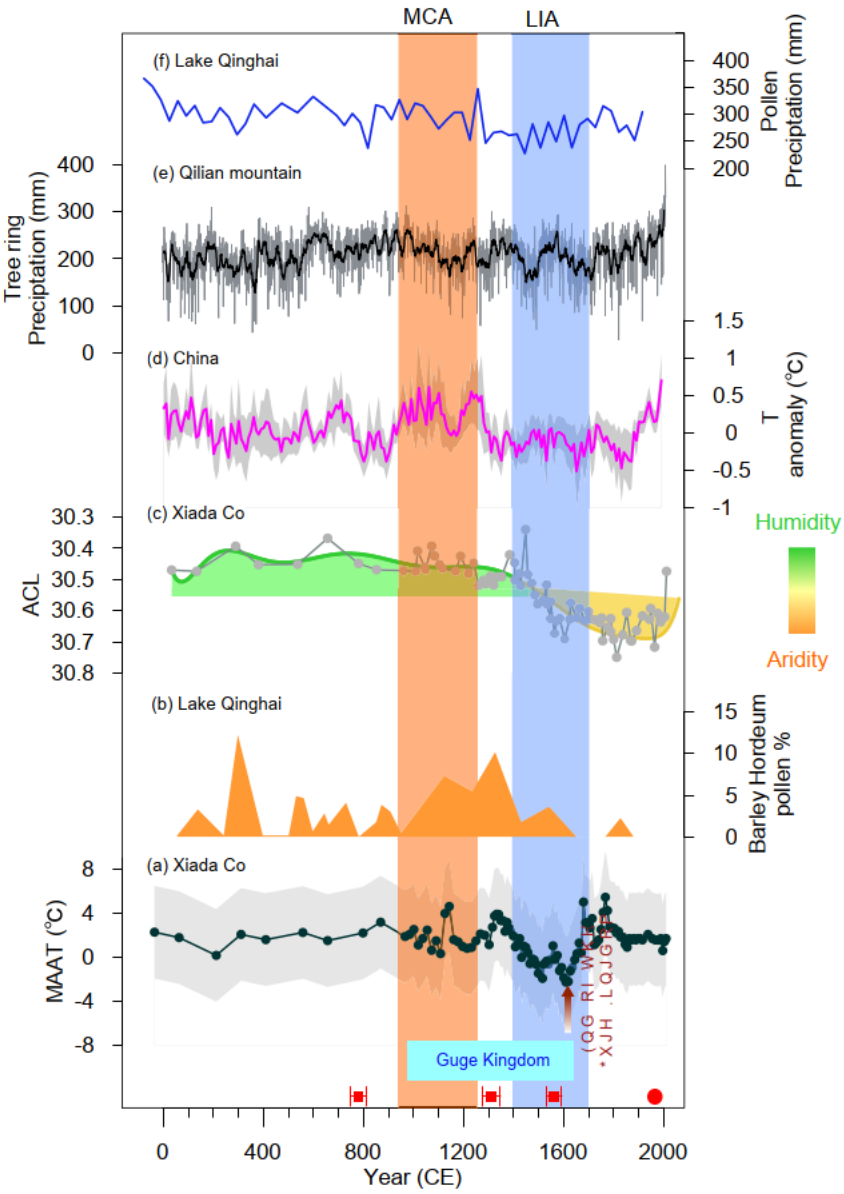

Figure 7. (a) Reconstructed MAAT using brGDGT in Xiada Co; (b) the pollen of Qingke barley Hordeum in Lake Qinghai, Tibet (Wei et al., 2020); (c) recalculated average long chain length (C30-32) value (ACL30-32) from n-alkanoic acid in Xiada Co (revised from Li et al., 2019); (d) composite document temperature records in China (Ge et al., 2013); precipitation

reconstructions from (e) tree rings in the Qilian mountains of north-eastern Tibet (Yang et al., 2014) and from (f) pollen in Lake Qinghai, Tibet (Lv et al., 2021).

Most archaeologists have argued that although the fall of the Guge Kingdom may have been affected by political factors, limited agriculture during this period could contribute to political instability and may be another potential reason which contributed to the breakup of the Guge Kingdom (Ryavec, 2015; Yuan, 2009). Ladakh, which is located to the north of Guge, won a war against Guge during the low temperature interval at ~1630 CE. Our analyses reveal that decreasing temperatures shrunk the area of Qingke barley in Guge, thus Ladakh would have had a larger available area for cultivation during the declining temperatures (Figs. 8e & 8f). This contrasts with observations of a negative relationship between the crop and temperature at decadal scales (Tsechoe *et al.*, 2021). This may be due to the optimum temperature for barley growth, as increasing temperature over the limit would certainly lead to a decline in yield. Our barley simulation clearly shows that if MAAT is below 0 °C, crop production would decrease (Fig.8d). A remote sensing survey showed the abandoned cultivated fields were once four times larger during the Guge Kingdom period than they currently span in Bedongpo valley, about thirty kilometers southeast of Guge (Ryavec, 2015). In addition, there is a supply-demand relationship between production of highland barley and population in the recent decade (Tsechoe *et al.*, 2021). Ryavec (2015) estimated per capita cultivated about ~0.11-hectare land in this region, suggesting Ladakh would have had a higher population and grain yields during the war. Besides temperature, decreased water level for agricultural irrigation in Guge could also have contributed to later declines in grain yields. From pollen records of western TP during the late Holocene, the *Artemisia*/*Chenopodiaceae* (A/C) ratio, which distinguishes moisture conditions, indicate a decrease of regional moisture (Li *et al.*, 2021b). The cold temperatures would have resulted in decreasing meltwater flow into the valley, which also led to significant lowering of water tables (Li *et al.*, 2019) and farmland abandonment.

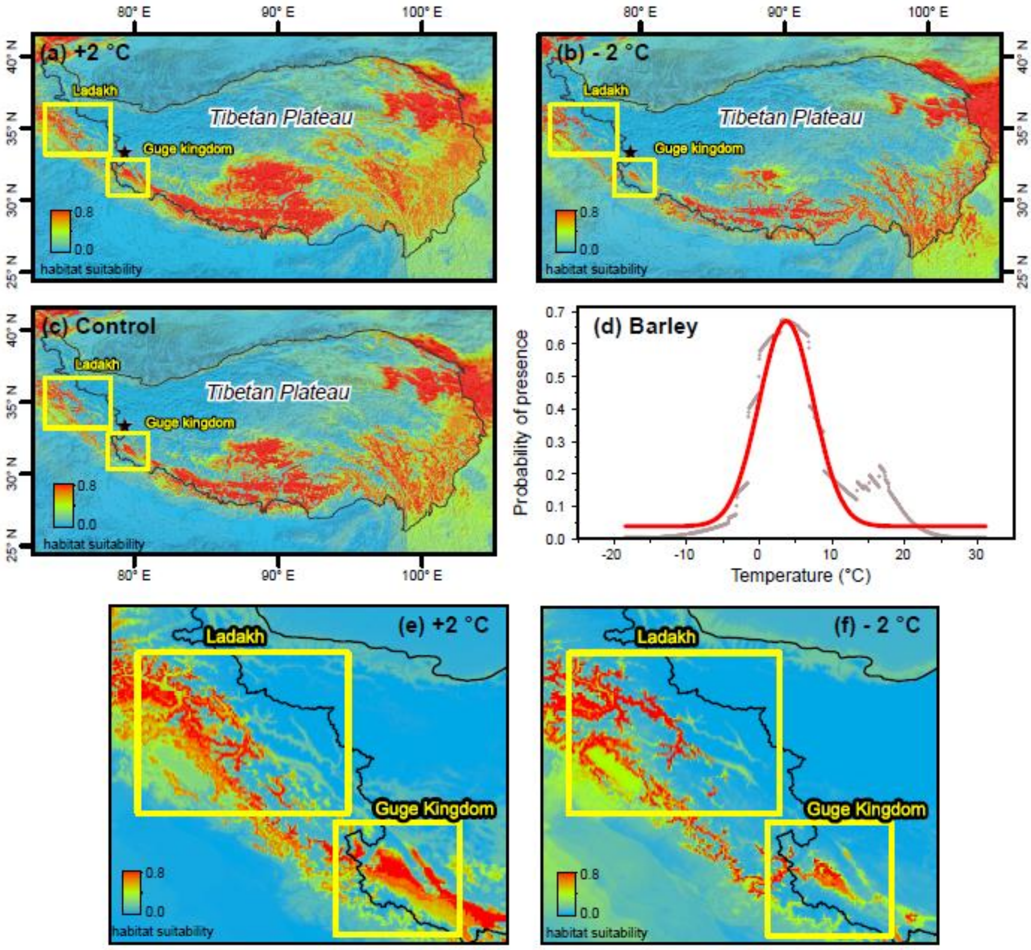

Figure 8. Maps showing the distribution and habitat suitability for Qingke barley. (a) increasing 2 °C and (b)decreasing 2 °C relative to (c) the modern scenario (control). (d) The plot shows the suitable temperature range for Qingke barley. This map shows the distribution and habitat suitability for of Qingke barley in the Ladakh and Guge Kingdom when temperatures are (e) increased by 2 °C and (f) decreased by 2 °C relative to the control.

Conclusions

We present a new Chinese lake MBT'_{6Me}-MAAT calibration based on 29 newly-measured samples along with 39 previously published samples from Chinese lakes. The temperature reconstructed from different lake types reveal that the extent of lake mixing influenced brGDGT-based temperatures. For example, brGDGT-derived temperatures represent annual lake bottom temperature or lake column temperature during mixing season in dimictic lakes but annual bottom water temperatures in meromictic lakes. We apply this new MBT'_{6Me}-MAAT calibration to a previously published sequence from dimictic lake Xiada Co, Western Tibet, China, and find that temperatures reconstructed from the top-most samples are consistent with lake bottom temperature and lake column temperatures during the mixing season. We translate this water temperature to air temperature and showed that the air temperature during LIA was 2 – 3 °C cooler than present, consistent with other paleoclimate records. Finally, we use ecological niche modelling to test the effect of temperature change on local agriculture. Our simulation suggests that decreasing temperatures, which contributed to diminishing crop production, were likely responsible for the collapse of the Guge Kingdom.

Acknowledgements

The authors would like to thank the editors and two anonymous reviewers for their contractive comments. We would like to thank Drs. Xiumei Li, Shaopeng Gao, Carrie Morrill, Yu Gao, Songtao Chen, Xiaoxia Li and Xianyong Cao for advice and analytical support. This study was supported by the Natural Science Foundation of China (Grant No. 42007409); the Strategic Priority Research Program of Chinese Academy of Sciences “Pan-third pole environmental change and the construction of green Silk Road” (Grant No. XDA20090000); International Partnership Program of Chinese Academy of Sciences (Grant No. 131C11KYSB20190035); and open foundation of MOE Key Laboratory of Western China's Environmental System and Basic Science Center for Tibetan Plateau Earth System (BSCTPES, Grant No. 41988101).

Open Research

Data generated in this study are available in National Tibetan Plateau Data Center (Liang, 2021). The previous published Chinese core-top brGDGTs are available through Dang *et al.* (2018); Lake 578 brGDGTs and monitored temperatures are available through Zhao *et al.* (2021), Xiada Co brGDGTs and the average chain length (ACL) of fatty acids are available at Li *et al.* (2019); global lake brGDGTs compiled by Martínez-Sosa *et al.* (2021) and Harning *et al.* (2020); Chinese soil brGDGTs compiled by Crampton-Flood *et al.* (2020), Duan *et al.* (2020) and Wang *et al.* (2020a). Dagze Co monitored temperatures are available through Wang *et al.* (2021a). MAAT reconstruction based on alkenones from Lake Qinghai is available through Hou *et al.* (2016); temperature proxy ($U_{37}^{k\prime}$) based on alkenones from lake Gahai and Sugan respectively are available through He *et al.* (2013); temperature anomaly reconstruction based on ice cores $\delta^{18}O$ from Chongce is available through Pang *et al.* (2020); changes in total solar irradiance are available through Schmidt *et al.* (2011) and volcanic forcing from tropical and Northern Hemisphere eruptions Sigl *et al.* (2015). The pollen of barley Hordeum in Lake Qinghai, Tibet is available through Wei *et al.* (2020); composite document temperature records in China is available through Ge *et al.* (2013); precipitation reconstructions from tree rings in the Qilian mountain is available through Yang *et al.* (2014) and pollen in Lake Qinghai, Tibet is available through Lv *et al.* (2021). Lake model simulated data for Xiada Co with ~37 year (1979–2015 CE) are available through Chen *et al.* (2011). The qingke barley simulation data were obtained through published field work (Zeng *et al.*, 2018) and the remainder of the data were sourced from the Global Biodiversity Information Facility (GBIF.org, 2019). The climatic variables (MAAT and annual precipitation) for species distribution modelling and brGDGTs analysis available through WorldClim2 database (https://www.worldclim.org/data/). Meteorological data set of Ngari Station were available through National Tibetan Plateau Data center (Zhao, 2018). Meteorological data from Shiquanhe, Gaize, Lazi, Bange and Shenzha station are available through China Meteorological Data service centre (http://data.cma.cn/).

Table

Table 1. Geographical and limnological data for 29 lakes studied, including latitude and longitude, elevation, surface area, lake depth, surface water pH, average lake water salinity and dissolved oxygen concentration (DO), lake surface temperature (LST), mean annual air temperatures (MAAT) and mixing types. The LST and DO were measured during field trip, MAAT is derived from WorldClim2 dataset. The n.d. means no data.

No	Lake name	Longitude (°N)	Latitude (°E)	Elevation (m)	Area (km^2)	Depth (m)	pH	Salinity (g/L)	DO (mg/g)	LST (°C)	MAAT (°C)
1	Anggu Co	85.4	31.2	4665	23	13	10	1.89	5.87	15.11	-0.35
2	Nairiping Co	91.43	31.32	4529	70	8	10	7.96	5.71	14.2	0.04
3	Gemang Co	87.28	31.58	4610	52	44	n.d.	6.35	5.92	14.3	0.85
4	Cuo Er1	88.7	31.67	4531	269	27	8	0.21	5.91	15	1.28
5	Qiagui Co	88.29	31.84	4645	91	26	10	0.22	6.29	14.4	1.11
6	Dagze Co	87.56	31.87	4470	245	34	10	14.42	5.42	15.3	0.31
7	Laguo Co	84.17	32.05	4471	91	18	9	40.27	4.71	16	0.13
8	Bieruoze Co	82.96	32.42	4413	33	2	9	27.38	4.6	15.67	0.14
9	Darebu Co	83.2	32.47	4441	21	3	n.d.	1.39	6.41	16.2	0.18
10	Rebang Co	80.51	33.04	4337	32		9	53.6	5.29	17	-0.22
11	Bangong Co	79.83	33.53	4244	604	38	9	0.5	6.4	15.6	-0.16
12	Jieze Caka	80.88	33.94	4512	108	36	n.d.	n.d.	n.d.	n.d.	-2.33
13	Songmuxi Co	80.23	34.6	5036	25	7	8	0.26	5.84	11.6	-6.64
14	Ga Hai	97.53	37.14	2854	47	9	8	n.d.	4.2	17	4.27
15	Xiaochaidan	95.44	37.52	3171	72	1	8	n.d.	4.3	15	1.69
16	Lake Sugan	94.22	39.07	2792	104	3	9	20	6	17	1.13
17	Beng Co	91.16	31.23	4829	141		9	0.16	7	10.3	-1.23
18	Cuo Er2	91.46	31.51	4494		1	9	3.63	6.08	14	-0.32
19	Cuona	91.45	32.08	4548	182	18	n.d.	0.27	6.65	12	-1.12
20	Daru Co	90.74	31.71	4690	54	10	8	5.05	6.44	12.8	-1.77
21	Xiada Co	79.37	33.4	4373	8	20	n.d.	0.15	6.9	8.5	-1.02
22	Dawa Co	84.97	31.25	4599	114	2	9	18.58	5.73	16.1	-1.04
23	Jiang Co	90.83	31.52	4603	36	22	10	14.6	5.98	12.5	-0.75
24	Lake Keluke	96.89	37.27	2840	57	6	8	0.66	7.09	17.6	3.93
25	Kongmu Co	90.44	29.01	4451	40	17	8	0.23	6.24	14.6	2.02
26	Kuhai	99.17	35.3	4132	49	10	9	16.1	6.51	8	-4.35
27	Peng Co	90.96	31.38	4569	136	8	9	8.54	6.29	11.7	-0.63
28	Lake Ranwu	96.78	29.47	3920	22	20	n.d.	n.d.	n.d.	n.d.	1.33
29	Zigetang Co	90.84	32.06	4575	191	15	10	13.5	5.87	13.5	-1.6

Table 2. Comparison of mean annual temperature (MAT), summer temperature (summer T) and mean temperature of months above freezing (MAF T) from station, lake water with reconstrued temperature (MAATre) using our MBT´$_{6Me}$-MAAT calibration. The station temperature for Dagze Co is derived from Shenzha meteorological station (available from the year of 1961 to 2016), Lake 578 is derived from meteorological station in Narsarsuaq (Zhao *et al.*, 2021; available from the year of 1961 to 2016) and Xiada Co is derived from Ali meteorological station (available from the year of 2010 to 2016). Lake column temperatures were calculated by monitored temperature for Dagze Co (Wang *et al.*, 2021b; from the year 2012 to 2015) and Lake 578 (Zhao *et al.*, 2021; from the year 2016 to 2019), and modelled temperature for Xiada Co (from the year 1979 to 2015). The lake bottom temperate is the last monitor set depth, Dagze Co was at 34 m (lake depth is 38 m) and Lake 578 was at 14 m (lake depth is 16 m), and we choose 16 m for Xiada Co (lake depth is 20 m) from the lake model.

		Lake name		
		Dagze Co	Lake 578	Xiada Co
Station	MAT	0.17	1.44	1.63
	Summer T	9.13	10.37	13.18
	MAF T	6.77	7.17	8.28
Lake column	MAT	4.85	5.70	4.25
	Summer	9.00	10.40	7.54
	MAF	8.03	8.88	6.30
	Mixing	-	5.24	3.31
Lake bottom water	MAT	2.86	5.04	2.19
	Summer	2.93	7.38	2.67
	MAF	2.89	6.89	2.94
	Mixing	-	5.18	3.12
Surface sediments	MAATre	2.36	6.81	0.40

References

Baxter, A. J., Hopmans, E. C., Russell, J. M., and Sinninghe Damsté, J. S. (2019), Bacterial GMGTs in East African lake sediments: Their potential as palaeotemperature indicators. *Geochimica et Cosmochimica Acta*, *259*, 155-169. https://doi.org/10.1016/j.gca.2019.05.039.

Blaga, C. I., Reichart, G.-J., Vissers, E. W., Lotter, A. F., Anselmetti, F. S., and Sinninghe Damsté, J. S. (2011), Seasonal changes in glycerol dialkyl glycerol tetraether concentrations and fluxes in a perialpine lake: Implications for the use of the TEX86 and BIT proxies. *Geochimica et Cosmochimica Acta*, *75*(21), 6416-6428. https://doi.org/10.1016/j.gca.2011.08.016.

Cao, J., Rao, Z., Shi, F., and Jia, G. (2020), Ice formation on lake surfaces in winter causes warm-season bias of lacustrine brGDGT temperature estimates. *Biogeosciences*, *17*(9), 2521-2536. https://doi.org/10.5194/bg-17-2521-2020.

Chen, F., Dong, G., Zhang, D. J., Liu, X. Y., Jia, X., An, C.-B. et al. (2015), Agriculture facilitated permanent human occupation of the Tibetan Plateau after 3600 BP. *science*, *347*(6219), 248-250. https://doi.org/10.1126/science.1259172.

Chen, F., Zhang, J., Liu, J., Cao, X., Hou, J., Zhu, L. et al. (2020), Climate change, vegetation history, and landscape responses on the Tibetan Plateau during the Holocene: a comprehensive review. *Quaternary Science Reviews*, *243*, 106444. https://doi.org/10.1016/j.quascirev.2020.106444

Chen, Y., Yang, K., He, J., Qin, J., Shi, J., Du, J. et al. (2011), Improving land surface temperature modeling for dry land of China. *Journal of Geophysical Research: Atmospheres*, *116*(D20). https://doi.org/10.1029/2011JD015921.

Crampton-Flood, E. D., Tierney, J. E., Peterse, F., Kirkels, F. M., and Sinninghe Damsté, J. S. (2020), BayMBT: A Bayesian calibration model for branched glycerol dialkyl glycerol tetraethers in soils and peats. *Geochimica et Cosmochimica Acta*, *268*, 142-159. https://doi.org/10.1016/j.gca.2019.09.043.

Dang, X., Yang, H., Naafs, B. D. A., Pancost, R. D., and Xie, S. (2016), Evidence of moisture control on the methylation of branched glycerol dialkyl glycerol tetraethers in semi-arid and arid soils. *Geochimica et Cosmochimica Acta*, *189*, 24-36. https://doi.org/10.1016/j.gca.2016.06.004.

Dang, X., Ding, W., Yang, H., Pancost, R. D., Naafs, B. D. A., Xue, J. et al. (2018), Different temperature dependence of the bacterial brGDGT isomers in 35 Chinese lake sediments compared to that in soils. *Organic Geochemistry*, *119*, 72-79. https://doi.org/10.1016/j.orggeochem.2018.02.008.

De Jonge, C., Stadnitskaia, A., Cherkashov, G., and Damsté, J. S. S. (2016), Branched glycerol dialkyl glycerol tetraethers and crenarchaeol record post-glacial sea level rise and shift in source of terrigenous brGDGTs in the Kara Sea (Arctic Ocean). *Organic Geochemistry*, *92*, 42-54. https://doi.org/10.1016/j.orggeochem.2012.10.004.

De Jonge, C., Hopmans, E. C., Zell, C. I., Kim, J.-H., Schouten, S., and Damsté, J. S. S. (2014), Occurrence and abundance of 6-methyl branched glycerol dialkyl glycerol tetraethers in soils: Implications for palaeoclimate reconstruction. *Geochimica et Cosmochimica Acta*, *141*, 97-112. https://doi.org/10.1016/j.gca.2014.06.013.

De Jonge, C., Radujković, D., Sigurdsson, B. D., Weedon, J. T., Janssens, I., and Peterse, F. (2019), Lipid biomarker temperature proxy responds to abrupt shift in the bacterial community composition in geothermally heated soils. *Organic Geochemistry*, *137*, 103897. https://doi.org/10.1016/j.orggeochem.2019.07.006.

De Jonge, C., Hopmans, E. C., Stadnitskaia, A., Rijpstra, W. I. C., Hofland, R., Tegelaar, E. et al. (2013), Identification of novel penta-and hexamethylated branched glycerol dialkyl glycerol tetraethers in peat using HPLC–MS2, GC–MS and GC–SMB-MS. *Organic geochemistry*, *54*, 78-82. https://doi.org/10.1016/j.orggeochem.2015.11.009.

Dee, S. G., Russell, J. M., Morrill, C., Chen, Z., and Neary, A. (2018), PRYSM v2.0: A Proxy System Model for Lacustrine Archives. *Paleoceanography and Paleoclimatology*, *33*(11), 1250-1269. https://doi.org/10.1029/2018PA003413.

Ding, S., Xu, Y., Wang, Y., He, Y., Hou, J., Chen, L. et al. (2015), Distribution of branched glycerol dialkyl glycerol tetraethers in surface soils of the Qinghai–Tibetan Plateau: implications of brGDGTs-based proxies in cold and dry regions. *Biogeosciences*, *12*(11), 3141-3151. https://doi.org/10.5194/bg-12-3141-2015.

Dong, L., Li, Q., Li, L., and Zhang, C. L. (2015), Glacial–interglacial contrast in MBT/CBT proxies in the South China Sea: Implications for marine production of branched GDGTs and continental teleconnection. *Organic Geochemistry*, *79*, 74-82. https://doi.org/10.1016/j.orggeochem.2014.12.008.

Duan, Y., Sun, Q., Werne, J. P., Yang, H., Jia, J., Wang, L. et al. (2020), Soil pH Dominates the Distributions of Both 5- and 6-Methyl Branched Tetraethers in Arid Regions. *Journal of Geophysical Research: Biogeosciences*, *125*(10), e2019JG005356. https://doi.org/10.1029/2019JG005356.

Dugerdil, L., Joannin, S., Peyron, O., Jouffroy-Bapicot, I., Vannière, B., Boldgiv, B. et al. (2021), Climate reconstructions based on GDGT and pollen surface datasets from Mongolia and Baikal area: calibrations and applicability to extremely cold–dry environments over the Late Holocene. *Climate of the Past*, *17*(3), 1199-1226. https://doi.org/10.5194/cp-17-1199-2021.

Feng, X., Zhao, C., D'Andrea, W. J., Liang, J., Zhou, A., and Shen, J. (2019), Temperature fluctuations during the Common Era in subtropical southwestern China inferred from brGDGTs in a remote alpine lake. *Earth and Planetary Science Letters*, *510*, 26-36. https://doi.org/10.1016/j.epsl.2018.12.028.

Fick, S. E., and Hijmans, R. J. (2017), WorldClim 2: new 1-km spatial resolution climate surfaces for global land areas. *International Journal of Climatology*, *37*(12), 4302-4315. https://doi.org/10.1002/joc.5086.

GBIF.org (2019), GBIF Occurrence Download https://doi.org/10.15468/dl.0cgwkh.

Ge, Q., Hao, Z., Zheng, J., and Shao, X. (2013), Temperature changes over the past 2000 yr in China and comparison with the Northern Hemisphere. *Clim. Past*, *9*(3), 1153-1160. 10.5194/cp-9-1153-2013.

Halamka, T. A., McFarlin, J. M., Younkin, A. D., Depoy, J., Dildar, N., and Kopf, S. H. (2021), Oxygen limitation can trigger the production of branched GDGTs in culture. *Geochemical Perspectives Letters*, *19*, 36-39. http://dx.doi.org/10.7185/geochemlet.2132.

Harning, D. J., Curtin, L., Geirsdóttir, Á., D'Andrea, W. J., Miller, G. H., and Sepúlveda, J. (2020), Lipid Biomarkers Quantify Holocene Summer Temperature and Ice Cap Sensitivity in Icelandic Lakes. *Geophysical Research Letters*, *47*(3), e2019GL085728. https://doi.org/10.1029/2019GL085728.

He, Y., Zhao, C., Wang, Z., Wang, H., Song, M., Liu, W. et al. (2013), Late Holocene coupled moisture and temperature changes on the northern Tibetan Plateau. *Quaternary Science Reviews*, *80*, 47-57. https://doi.org/10.1016/j.quascirev.2013.08.017.

Hopmans, E. C., Schouten, S., and Sinninghe Damsté, J. S. (2016), The effect of improved chromatography on GDGT-based palaeoproxies. *Organic Geochemistry*, *93*, 1-6. https://doi.org/10.1016/j.orggeochem.2015.12.006.

Hostetler, S. W., and Bartlein, P. J. (1990), Simulation of lake evaporation with application to modeling lake level variations of Harney‐Malheur Lake, Oregon. *Water Resources Research*, *26*(10), 2603-2612. https://doi.org/10.1029/90WR01240.

Hou, J., Huang, Y., Zhao, J., Liu, Z., Colman, S., and An, Z. (2016), Large Holocene summer temperature oscillations and impact on the peopling of the northeastern Tibetan Plateau. *Geophysical Research Letters*, *43*(3), 1323-1330. https://doi.org/10.1002/2015GL067317.

Hou, S., Zhang, W., Pang, H., Wu, S.-Y., Jenk, T. M., Schwikowski, M. et al. (2019), Apparent discrepancy of Tibetan ice core δ 18 O records may be attributed to misinterpretation of chronology. *The Cryosphere*, *13*(6), 1743-1752. https://doi.org/10.5194/tc-13-1743-2019.

Hu, J., Zhou, H., and Spiro, B. (2016), Seasonal variability in concentrations and fluxes of glycerol dialkyl glycerol tetraethers in Huguangyan Maar Lake, SE China: Implications for the applicability of the MBT–CBT paleotemperature proxy in lacustrine settings. *Chemical Geology*, *420*, 200-212. https://doi.org/10.1016/j.chemgeo.2015.11.008.

Hutter, K., Chubarenko, I. P., and Wang, Y. (2014), *Physics of Lakes: Volume 3: Methods of Understanding Lakes as Components of the Geophysical Environment*. Heidelberg: Springer.

Joshi, P., Phartiyal, B., and Joshi, M. (2021), Hydro-climatic variability during last five thousand years and its impact on human colonization and cultural transition in Ladakh sector, India. *Quaternary International*, *599*, 45-54. https://doi.org/10.1016/j.quaint.2020.09.053.

Kathayat, G., Cheng, H., Sinha, A., Yi, L., Li, X., Zhang, H. et al. (2017), The Indian monsoon variability and civilization changes in the Indian subcontinent. *Science advances*, *3*(12), e1701296. https://doi.org/10.1126/sciadv.1701296.

Katsev, S., Verburg, P., Llirós, M., Minor, E. C., Kruger, B. R., and Li, J. (2017), Tropical meromictic lakes: specifics of meromixis and case studies of Lakes Tanganyika, Malawi, and Matano, in *Ecology of Meromictic Lakes*, edited, pp. 277-323, Springer.

Kuhn, M. (2021), caret: Classification and Regression Training, edited.

Lei, Y., Yang, H., Dang, X., Zhao, S., and Xie, S. (2016), Absence of a significant bias towards summer temperature in branched tetraether-based paleothermometer at two soil sites with contrasting temperature seasonality. *Organic Geochemistry*, *94*, 83-94. https://doi.org/10.1016/j.orggeochem.2016.02.003.

Lewis Jr, W. M. (1973), The thermal regime of Lake Lanao (Philippines) and its theoretical implications for Tropical Lakes 1. *Limnology and Oceanography*, *18*(2), 200-217. https://doi.org/10.4319/lo.1973.18.2.0200.

Li, T.-Y., Wu, Y., Shen, C.-C., Li, J.-Y., Chiang, H.-W., Lin, K. et al. (2021a), High precise dating on the variation of the Asian summer monsoon since 37 ka BP. *Scientific reports*, *11*(1), 1-14. https://doi.org/10.1038/s41598-021-88597-7.

Li, X., Wang, M., and Hou, J. (2019), Centennial-scale climate variability during the past 2000 years derived from lacustrine sediment on the western Tibetan Plateau. *Quaternary International*, *510*, 65-75. https://doi.org/10.1016/j.quaint.2018.12.018.

Li, X., Wang, M., Zhang, Y., Lei, L., and Hou, J. (2017), Holocene climatic and environmental change on the western Tibetan Plateau revealed by glycerol dialkyl glycerol tetraethers and leaf wax deuterium-to-hydrogen ratios at Aweng Co. *Quaternary Research*, *87*(3), 455-467.

https://doi.org/10.1017/qua.2017.9.
Li, Z., Wang, Y., Herzschuh, U., Cao, X., Ni, J., and Zhao, Y. (2021b), Pollen-based mapping of Holocene vegetation on the Qinghai-Tibetan Plateau in response to climate change. *Palaeogeography, Palaeoclimatology, Palaeoecology*, *573*, 110412. https://doi.org/10.1016/j.palaeo.2021.110412.
Liang, J. (2021), BrGDGT data sets of lake surface sediments and settling particles from Dagze Co in Qinghai Tibet Plateau. National Tibetan Plateau Data Center, [Dataset] DOI: 10.11888/Paleoenv.tpdc.271728. CSTR: 18406.11.Paleoenv.tpdc.271728.
Liang, J., Russell, J. M., Xie, H., Lupien, R. L., Si, G., Wang, J. et al. (2019), Vegetation effects on temperature calibrations of branched glycerol dialkyl glycerol tetraether (brGDGTs) in soils. *Organic Geochemistry*, *127*, 1-11. https://doi.org/10.1016/j.orggeochem.2018.10.010.
Longo, W. M., Huang, Y., Russell, J. M., Morrill, C., Daniels, W. C., Giblin, A. E. et al. (2020), Insolation and greenhouse gases drove Holocene winter and spring warming in Arctic Alaska. *Quaternary Science Reviews*, *242*, 106438. https://doi.org/10.1016/j.quascirev.2020.106438.
Loomis, S. E., Russell, J. M., Heureux, A. M., D'Andrea, W. J., and Damsté, J. S. S. (2014), Seasonal variability of branched glycerol dialkyl glycerol tetraethers (brGDGTs) in a temperate lake system. *Geochimica et Cosmochimica Acta*, *144*, 173-187. https://doi.org/10.1016/j.gca.2014.08.027.
Lv, F., Chen, J., Zhou, A., Cao, X., Zhang, X., Wang, Z. et al. (2021), Vegetation History and Precipitation Changes in the NE Qinghai‐Tibet Plateau: A 7,900‐years Pollen Record From Caodalian Lake. *Paleoceanography and Paleoclimatology*, *36*(4), e2020PA004126. https://doi.org/10.1029/2020PA004126.
Martínez-Sosa, P., and Tierney, J. E. (2019), Lacustrine brGDGT response to microcosm and mesocosm incubations. *Organic Geochemistry*, *127*, 12-22. https://doi.org/10.1016/j.orggeochem.2018.10.011.
Martínez-Sosa, P., Tierney, J. E., Stefanescu, I. C., Dearing Crampton-Flood, E., Shuman, B. N., and Routson, C. (2021), A global Bayesian temperature calibration for lacustrine brGDGTs. *Geochimica et Cosmochimica Acta*, *305*, 87-105. https://doi.org/10.1016/j.gca.2021.04.038.
Merow, C., Smith, M. J., and Silander Jr, J. A. (2013), A practical guide to MaxEnt for modeling species' distributions: what it does, and why inputs and settings matter. *Ecography*, *36*(10), 1058-1069. https://doi.org/10.1111/j.1600-0587.2013.07872.x.
Miller, D. R., Habicht, M. H., Keisling, B. A., Castañeda, I. S., and Bradley, R. S. (2018), A 900-year New England temperature reconstruction from in situ seasonally produced branched glycerol dialkyl glycerol tetraethers (brGDGTs). *Climate of the Past*, *14*(11), 1653-1667. https://doi.org/10.5194/cp-14-1653-2018.
Mudelsee, M. (2000), Ramp function regression: a tool for quantifying climate transitions. *Computers & Geosciences*, *26*(3), 293-307. https://doi.org/10.1016/S0098-3004(99)00141-7.
Naafs, B., Gallego-Sala, A., Inglis, G., and Pancost, R. (2017a), Refining the global branched glycerol dialkyl glycerol tetraether (brGDGT) soil temperature calibration. *Organic Geochemistry*, *106*, 48-56. https://doi.org/10.1016/j.orggeochem.2017.01.009.
Naafs, B., McCormick, D., Inglis, G., and Pancost, R. (2018), Archaeal and bacterial H-GDGTs are abundant in peat and their relative abundance is positively correlated with temperature. *Geochimica et Cosmochimica Acta*, *227*, 156-170. https://doi.org/10.1016/j.gca.2018.02.025.
Naafs, B. D. A., Inglis, G. N., Zheng, Y., Amesbury, M., Biester, H., Bindler, R. et al. (2017b),

Introducing global peat-specific temperature and pH calibrations based on brGDGT bacterial lipids. *Geochimica et Cosmochimica Acta*, *208*, 285-301. https://doi.org/10.1016/j.gca.2017.01.038.

Oksanen, J., Blanchet, F. G., Friendly, M., Kindt, R., Legendre, P., McGlinn, D. et al. (2020), vegan: Community Ecology Package, *URL: https://CRAN.R-project.org/package=vegan*

Pang, H., Hou, S., Zhang, W., Wu, S., Jenk, T. M., Schwikowski, M. et al. (2020), Temperature Trends in the Northwestern Tibetan Plateau Constrained by Ice Core Water Isotopes Over the Past 7,000 Years. *Journal of Geophysical Research: Atmospheres*, *125*(19), e2020JD032560. https://doi.org/10.1029/2020JD032560.

Peterse, F., van der Meer, J., Schouten, S., Weijers, J. W., Fierer, N., Jackson, R. B. et al. (2012), Revised calibration of the MBT–CBT paleotemperature proxy based on branched tetraether membrane lipids in surface soils. *Geochimica et Cosmochimica Acta*, *96*, 215-229. https://doi.org/10.1016/j.gca.2012.08.011.

Phillips, S. J., Dudík, M., and Schapire, R. E. (2017), Maxent software for modeling species niches and distributions (Version 3.4. 1). *Biodiversity Informatics*. Available from url: http://biodiversityinformatics.amnh.org/open_source/maxent/. Accessed on 2022-3-2.

Qiu, J. (2008), China: the third pole. *Nature News*, *454*(7203), 393-396. https://doi.org/10.1038/454393a.

R Core Team (2021), R: A language and environment for statistical computing, edited, R Foundation for Statistical Computing, Vienna, Austria.

Raberg, J. H., Harning, D. J., Crump, S. E., de Wet, G., Blumm, A., Kopf, S. et al. (2021), Revised fractional abundances and warm-season temperatures substantially improve brGDGT calibrations in lake sediments. *Biogeosciences*, *18*(12), 3579-3603. https://doi.org/10.5194/bg-18-3579-2021.

Russell, J. M., Hopmans, E. C., Loomis, S. E., Liang, J., and SinningheDamsté, J. S. (2018), Distributions of 5-and 6-methyl branched glycerol dialkyl glycerol tetraethers (brGDGTs) in East African lake sediment: Effects of temperature, pH, and new lacustrine paleotemperature calibrations. *Organic Geochemistry*, *117*, 56-69. https://doi.org/10.1016/j.orggeochem.2017.12.003.

Ryavec, K. E. (2015), *A historical atlas of Tibet*: University of Chicago Press.

Schmidt, G. A., Jungclaus, J. H., Ammann, C., Bard, E., Braconnot, P., Crowley, T. et al. (2011), Climate forcing reconstructions for use in PMIP simulations of the last millennium (v1. 0). *Geoscientific Model Development*, *4*(1), 33-45. https://doi.org/10.5194/gmd-4-33-2011.

Sigl, M., Winstrup, M., McConnell, J. R., Welten, K. C., Plunkett, G., Ludlow, F. et al. (2015), Timing and climate forcing of volcanic eruptions for the past 2,500 years. *Nature*, *523*(7562), 543-549. https://doi.org/10.1038/nature14565.

Sinninghe Damsté, J. S., Hopmans, E. C., Pancost, R. D., Schouten, S., and Geenevasen, J. A. (2000), Newly discovered non-isoprenoid glycerol dialkyl glycerol tetraether lipids in sediments. *Chemical Communications*(17), 1683-1684. https://doi.org/10.1039/b004517i.

Stefanescu, I. C., Shuman, B. N., and Tierney, J. E. (2021), Temperature and water depth effects on brGDGT distributions in sub-alpine lakes of mid-latitude North America. *Organic Geochemistry*, *152*, 104174. https://doi.org/10.1016/j.orggeochem.2020.104174.

Tang, X., Naafs, B. D. A., Pancost, R. D., Liu, Z., Fan, T., and Zheng, Y. (2021), Exploring the influences of temperature on "H-Shaped" Glycerol Dialkyl Glycerol Tetraethers in a stratigraphic context: evidence from two peat cores across the late Quaternary. *Frontiers in Earth Science*, *8*, 477. https://doi.org/10.3389/feart.2020.541685.

Tsechoe, D., Piao, S., Wang, X., Zhao, C., Liu, B., Chen, A. et al. (2021), Emerging negative warming impacts on tibetan crop yield. *Engineering*. https://doi.org/10.1016/j.eng.2021.01.012.

Van Bree, L. G. J., Peterse, F., Baxter, A. J., De Crop, W., van Grinsven, S., Villanueva, L. et al. (2020), Seasonal variability and sources of in situ brGDGT production in a permanently stratified African crater lake. *Biogeosciences*, *17*(21), 5443-5463. https://doi.org/10.5194/bg-17-5443-2020.

Wang, H., Liu, W., and Lu, H. (2016), Appraisal of branched glycerol dialkyl glycerol tetraether-based indices for North China. *Organic Geochemistry*, *98*, 118-130. https://doi.org/10.1016/j.orggeochem.2016.05.013.

Wang, H., An, Z., Lu, H., Zhao, Z., and Liu, W. (2020a), Calibrating bacterial tetraether distributions towards in situ soil temperature and application to a loess-paleosol sequence. *Quaternary Science Reviews*, *231*, 106172. https://doi.org/10.1016/j.quascirev.2020.106172.

Wang, M., Hou, J., and Lei, Y. (2014), Classification of Tibetan lakes based on variations in seasonal lake water temperature. *Chinese Science Bulletin*, *59*(34), 4847-4855. https://doi.org/10.1007/s11434-014-0588-8.

Wang, M., Tian, Q., Li, X., Liang, J., He, Y., and Hou, J. (2020b), TEX86 as a potential proxy of lake water pH in the Tibetan Plateau. *Palaeogeography, Palaeoclimatology, Palaeoecology*, *538*, 109381. https://doi.org/10.1016/j.palaeo.2019.109381.

Wang, M., Hou, J., Lazhu, Li, X., Liang, J., Xie, S. et al. (2021a), Changes in the lake thermal and mixing dynamics on the Tibetan Plateau. *Hydrological Sciences Journal*, *66*(5), 838-850. https://doi.org/10.1080/02626667.2021.1887487.

Wang, M., Hou, J., Duan, Y., Chen, J., Li, X., He, Y. et al. (2021b), Internal feedbacks forced Middle Holocene cooling on the Qinghai-Tibetan Plateau. *Boreas*, *n/a*(n/a). https://doi.org/10.1111/bor.12531.

Weber, Y., De Jonge, C., Rijpstra, W. I. C., Hopmans, E. C., Stadnitskaia, A., Schubert, C. J. et al. (2015), Identification and carbon isotope composition of a novel branched GDGT isomer in lake sediments: Evidence for lacustrine branched GDGT production. *Geochimica et Cosmochimica Acta*, *154*, 118-129. https://doi.org/10.1073/pnas.1805186115.

Weber, Y., Damsté, J. S. S., Zopfi, J., De Jonge, C., Gilli, A., Schubert, C. J. et al. (2018), Redox-dependent niche differentiation provides evidence for multiple bacterial sources of glycerol tetraether lipids in lakes. *Proceedings of the National Academy of Sciences*, *115*(43), 10926-10931. https://doi.org/10.1073/pnas.1805186115.

Wei, H., E, C., Zhang, J., Sun, Y., Li, Q., Hou, G. et al. (2020), Climate change and anthropogenic activities in Qinghai Lake basin over the last 8500 years derived from pollen and charcoal records in an aeolian section. *CATENA*, *193*, 104616. https://doi.org/10.1016/j.catena.2020.104616.

Weijers, J. W., Schouten, S., van den Donker, J. C., Hopmans, E. C., and Sinninghe Damsté, J. S. (2007), Environmental controls on bacterial tetraether membrane lipid distribution in soils. *Geochimica et Cosmochimica Acta*, *71*(3), 703-713. https://doi.org/10.1016/j.gca.2006.10.003.

Weijers, J. W., Schouten, S., Hopmans, E. C., Geenevasen, J. A., David, O. R., Coleman, J. M. et al. (2006), Membrane lipids of mesophilic anaerobic bacteria thriving in peats have typical archaeal traits. *Environmental Microbiology*, *8*(4), 648-657. https://doi.org/10.1111/j.1462-2920.2005.00941.x.

Woolway, R. I., and Merchant, C. J. (2019), Worldwide alteration of lake mixing regimes in response to climate change. *Nature Geoscience*, *12*(4), 271-276. https://doi.org/10.1038/s41561-019-0322-x.

Wu, J., Yang, H., Pancost, R. D., Naafs, B. D. A., Qian, S., Dang, X. et al. (2021), Variations in dissolved O_2 in a Chinese lake drive changes in microbial communities and impact sedimentary GDGT distributions. *Chemical Geology*, 120348. https://doi.org/10.1016/j.chemgeo.2021.120348.

Xiao, W., Xu, Y., Ding, S., Wang, Y., Zhang, X., Yang, H. et al. (2015), Global calibration of a novel, branched GDGT-based soil pH proxy. *Organic Geochemistry*, *89-90*, 56-60. https://doi.org/10.1016/j.orggeochem.2015.10.005.

Xie, H., Liang, J., Vachula, R. S., Russell, J. M., Chen, S., Guo, M. et al. (2021), Changes in the hydrodynamic intensity of Bosten Lake and its impact on early human settlement in the northeastern Tarim Basin, Arid Central Asia. *Palaeogeography, Palaeoclimatology, Palaeoecology*, 110499. https://doi.org/10.1016/j.palaeo.2021.110499.

Yang, B., Qin, C., Wang, J., He, M., Melvin, T. M., Osborn, T. J. et al. (2014), A 3,500-year tree-ring record of annual precipitation on the northeastern Tibetan Plateau. *Proceedings of the National Academy of Sciences*, *111*(8), 2903-2908. https://doi.org/10.1073/pnas.1319238111.

Yang, H., Lü, X., Ding, W., Lei, Y., Dang, X., and Xie, S. (2015), The 6-methyl branched tetraethers significantly affect the performance of the methylation index (MBT′) in soils from an altitudinal transect at Mount Shennongjia. *Organic Geochemistry*, *82*, 42-53. https://doi.org/10.1016/j.orggeochem.2015.02.003.

Yao, T., Xue, Y., Chen, D., Chen, F., Thompson, L., Cui, P. et al. (2019), Recent third pole's rapid warming accompanies cryospheric melt and water cycle intensification and interactions between monsoon and environment: Multidisciplinary approach with observations, modeling, and analysis. *Bulletin of the American Meteorological Society*, *100*(3), 423-444. https://doi.org/10.1175/BAMS-D-17-0057.1.

Yao, Y., Zhao, J., Vachula, R. S., Werne, J. P., Wu, J., Song, X. et al. (2020), Correlation between the ratio of 5-methyl hexamethylated to pentamethylated branched GDGTs (HP5) and water depth reflects redox variations in stratified lakes. *Organic Geochemistry*, *147*, 104076. https://doi.org/10.1016/j.orggeochem.2020.104076.

Yuan, H.-S., Wei, Y.-L., and Wang, X.-G. (2015), Maxent modeling for predicting the potential distribution of Sanghuang, an important group of medicinal fungi in China. *Fungal Ecology*, *17*, 140-145. https://doi.org/10.1016/j.funeco.2015.06.001.

Yuan, S. (2009), The Mystery of the Guge Kingdom in Tibet, in *China Religious Culture Publisher*, edited.

Zadereev, E. S., Boehrer, B., and Gulati, R. D. (2017), Introduction: meromictic lakes, their terminology and geographic distribution, in *Ecology of Meromictic lakes*, edited, pp. 1-11, Springer.

Zeng, X., Guo, Y., Xu, Q., Mascher, M., Guo, G., Li, S. et al. (2018), Origin and evolution of qingke barley in Tibet. *Nature Communications*, *9*(1), 1-11. https://doi.org/10.1038/s41467-018-07920-5.

Zhang, C., Zhao, C., Yu, S.-Y., Yang, X., Cheng, J., Zhang, X. et al. (2022), Seasonal imprint of Holocene temperature reconstruction on the Tibetan Plateau. *Earth-Science Reviews*, 103927. https://doi.org/10.1016/j.earscirev.2022.103927.

Zhang, C., Zhao, C., Zhou, A., Zhang, H., Liu, W., Feng, X. et al. (2021), Quantification of temperature and precipitation changes in northern China during the "5000-year" Chinese History. *Quaternary Science Reviews*, *255*, 106819. https://doi.org/10.1016/j.quascirev.2021.106819.

Zhao, B., Castañeda, I. S., Bradley, R. S., Salacup, J. M., de Wet, G. A., Daniels, W. C. et al. (2021), Development of an in situ branched GDGT calibration in Lake 578, southern Greenland. *Organic Geochemistry*, *152*, 104168. https://doi.org/10.1016/j.orggeochem.2020.104168.

Zhao, B., Castañeda Isla, S., Salacup Jeffrey, M., Thomas Elizabeth, K., Daniels William, C., Schneider, T. et al. (2022), Prolonged drying trend coincident with the demise of Norse settlement in southern Greenland. *Science Advances*, *8*(12), eabm4346. https://doi.org/10.1126/sciadv.abm4346.

Zhao, H. (2018), Meteorological data of the integrated observation and research station of Ngari for desert environment (2009-2017). National Tibetan Plateau Data Center, [Dataset] DOI: 10.11888/AtmosphericPhysics.tpe.62.db. CSTR: 18406.11.AtmosphericPhysics.tpe.62.db.

Supplementary information for

Calibration and application of branched GDGTs to Tibetan lake sediments: the influence of temperature on the fall of the Guge Kingdom in Western Tibet, China

Jie Liang[1,2], Yanlong Guo[3], Nora Richter[4], Haichao Xie[1], Richard S. Vachula[5], Rachel L. Lupien[6], Boyang Zhao[2], Mingda Wang[7], Yuan Yao[8], Juzhi Hou[1], Jianbao Liu[1], James M. Russell[2]

[1]Group of Alpine Paleoecology and Human Adaptation (ALPHA), State Key Laboratory of Tibetan Plateau Earth System, Resources and Environment (TPESRE), Institute of Tibetan Plateau Research, Chinese Academy of Sciences, Beijing, China, [2]Department of Earth, Environmental, and Planetary Sciences, Brown University, Providence, USA, [3]National Tibetan Plateau Data Center, Key Laboratory of Tibetan Environmental Changes and Land Surface Processes, Institute of Tibetan Plateau Research, Beijing, China , [4]NIOZ Royal Institute for Sea Research, Department of Marine Microbiology and Biogeochemistry, , Texel, The Netherlands, [5]Department of Geology, College of William and Mary, Williamsburg, USA, [6]Division of Biology and Paleo Environment, Lamont-Doherty Earth Observatory, Palisades, USA, [7]School of Geography, Liaoning Normal University, Dalian, China, [8]Institute of Global Environmental Change, Xi'an Jiaotong University, Xi'an, China

Contents of this file

Table S1. Relative abundance of brGDGTs form Chinese lake surface sediments (Dang *et al.*, 2018 and this study) used in our new calibration.

ID	Lake name	Lat (°N)	Long (°E)	IIIa	IIIa'	IIIb	IIIb'	IIIc	IIIc'	IIa	IIa'	IIb	IIb'	IIc	IIc'	Ia	Ib	Ic	References
1	Anggu Co	31.2	85.4	0.07	0.32	0	0	0	0	0.09	0.27	0	0.1	0	0	0.15	0	0	This study
2	Bangong Co	33.53	79.83	0.14	0.34	0.01	0.03	0.01	0	0.06	0.15	0.06	0.08	0.01	0	0.07	0.03	0.01	This study
3	Beng Co	31.23	91.16	0.25	0.4	0	0	0	0	0.08	0.11	0.06	0.04	0	0	0.07	0	0	This study
4	Bieruoze Co	32.42	82.96	0.08	0.23	0	0	0	0	0.08	0.24	0.04	0.11	0	0	0.14	0.08	0	This study
5	Cuo Er	31.67	88.7	0.04	0.53	0	0	0	0	0.03	0.24	0.01	0.04	0	0	0.08	0.02	0	This study
6	Cuo Er2	31.51	91.46	0.2	0.11	0.02	0.04	0	0	0.1	0.2	0.06	0.09	0	0	0.13	0.04	0	This study
7	Cuo Na	32.08	91.45	0.14	0.35	0.03	0.06	0.01	0.02	0.07	0.11	0.05	0.09	0.01	0.01	0.04	0.02	0	This study
8	Darebu Co	32.47	83.2	0.13	0.19	0	0	0	0	0.11	0.26	0.04	0.08	0	0	0.14	0.04	0	This study
9	Daru Co	31.71	90.74	0.13	0.19	0	0	0	0	0.11	0.26	0.04	0.08	0	0	0.14	0.04	0	This study
10	Dawa Co	31.25	84.97	0.13	0.22	0	0	0	0	0.13	0.22	0.05	0.09	0	0	0.1	0.05	0	This study
11	Dagze Co	31.87	87.56	0.11	0.15	0	0	0	0	0.08	0.25	0.05	0.16	0.01	0.03	0.1	0.07	0	This study
12	Gai Hai	37.14	97.53	0.05	0.2	0	0	0	0	0.08	0.24	0.07	0.1	0	0	0.15	0.08	0.03	This study
13	Gemang Co	31.58	87.28	0.06	0.23	0	0	0	0	0.07	0.27	0.05	0.1	0.01	0.02	0.13	0.05	0.01	This study
14	Jiang Co	31.52	90.83	0.12	0.26	0	0	0	0	0.11	0.21	0.05	0.08	0	0	0.12	0.05	0	This study
15	Jieze Chaka	33.94	80.88	0.04	0.13	0	0	0	0.06	0.02	0.11	0.02	0.27	0	0.23	0.06	0.03	0.03	This study
16	Lake Keluke	37.27	96.89	0.18	0.11	0.02	0.01	0	0	0.12	0.17	0.1	0.06	0.01	0	0.14	0.07	0.01	This study

ID	Lake name	Lat (°N)	Long (°E)	IIIa	IIIa'	IIIb	IIIb'	IIIc	IIIc'	IIa	IIa'	IIb	IIb'	IIc	IIc'	Ia	Ib	Ic	References
17	Kongmu Co	29.01	90.44	0.21	0.18	0.03	0.02	0	0	0.09	0.13	0.12	0.06	0.01	0.01	0.07	0.04	0.02	This study
18	Ku Hai	35.3	99.17	0.11	0.15	0	0	0	0	0.11	0.18	0.12	0.12	0	0	0.12	0.09	0	This study
19	Laguo Co	32.05	84.17	0.06	0.25	0	0.05	0	0.04	0.03	0.16	0.02	0.14	0	0.05	0.16	0.04	0	This study
20	Nairiping Co	31.32	91.43	0.09	0.24	0	0	0	0	0.11	0.25	0.03	0.05	0	0	0.18	0.04	0	This study
21	Peng Co	31.38	90.96	0.13	0.33	0	0	0	0	0.1	0.25	0.03	0.06	0	0	0.08	0.02	0	This study
22	Qiagui Co	31.84	88.29	0.34	0.23	0.01	0.02	0	0	0.09	0.15	0.05	0.04	0	0	0.05	0.01	0	This study
23	Lake Ranwu	29.47	96.78	0.14	0.16	0.01	0.02	0	0.01	0.2	0.14	0.04	0.06	0.01	0.01	0.13	0.05	0.01	This study
24	Rebang Co	33.04	80.51	0.09	0.1	0.01	0.01	0	0	0.07	0.21	0.03	0.05	0.01	0.01	0.36	0.04	0	This study
25	Songmuxi Co	34.6	80.23	0.15	0.43	0.02	0.05	0.01	0.03	0.04	0.11	0.03	0.07	0.01	0.01	0.04	0.01	0	This study
26	Lake Sugan	39.07	94.22	0.07	0.11	0	0	0	0	0.12	0.21	0.05	0.05	0	0	0.33	0.06	0	This study
27	Xiada Co	33.4	79.37	0.22	0.22	0.02	0.01	0	0	0.11	0.17	0.09	0.03	0.01	0	0.09	0.02	0	This study
28	Xiaochaidan	37.52	95.44	0.11	0.26	0	0	0	0	0.12	0.19	0.05	0.13	0	0	0.07	0.06	0	This study
29	Zigetang Co	32.06	90.84	0.13	0.16	0	0	0	0	0.09	0.24	0.04	0.11	0	0	0.15	0.08	0	This study
30	Baiyangdian	38.93	115.99	0.05	0.08	0.01	0.01	0	0	0.16	0.18	0.08	0.06	0.01	0	0.22	0.12	0.02	(Dang et al., 2018)
31	Cetian	39.97	113.77	0.1	0.11	0.01	0.01	0	0	0.12	0.26	0.06	0.08	0.01	0.01	0.15	0.07	0.01	(Dang et al., 2018)
32	Daihai 1	40.58	112.67	0.04	0.11	0.01	0.01	0.01	0	0.07	0.11	0.08	0.09	0.02	0	0.11	0.25	0.09	(Dang et al., 2018)
33	Daihai 2	40.58	112.66	0.06	0.12	0.01	0.01	0	0	0.1	0.2	0.09	0.09	0.01	0	0.14	0.12	0.04	(Dang et al., 2018)
34	Daihai 3	40.59	112.65	0.06	0.11	0.01	0.01	0	0	0.1	0.22	0.07	0.1	0.01	0	0.14	0.12	0.04	(Dang et al., 2018)

ID	Lake name	Lat (°N)	Long (°E)	IIIa	IIIa'	IIIb	IIIb'	IIIc	IIIc'	IIa	IIa'	IIb	IIb'	IIc	IIc'	Ia	Ib	Ic	References
35	Dalongwan	42.34	126.39	0.08	0.08	0	0.01	0	0	0.26	0.16	0.06	0.04	0	0	0.21	0.08	0.01	(Dang et al., 2018)
36	Erlongwan	42.3	126.38	0.05	0.05	0	0	0	0	0.25	0.15	0.03	0.03	0.01	0	0.34	0.07	0.01	(Dang et al., 2018)
37	Fenghe	34.33	108.74	0.04	0.1	0.01	0.01	0	0	0.12	0.19	0.06	0.1	0.01	0.01	0.2	0.12	0.02	(Dang et al., 2018)
38	Guanting	40.37	115.76	0.1	0.12	0.01	0.01	0	0	0.14	0.23	0.09	0.07	0.01	0	0.13	0.08	0.01	(Dang et al., 2018)
39	Lake Caizi	30.79	117.1	0.05	0.04	0.01	0	0	0	0.19	0.13	0.09	0.04	0.01	0	0.26	0.15	0.02	(Dang et al., 2018)
40	Lake Chagan	45.21	124.33	0.07	0.14	0.01	0.01	0	0	0.11	0.28	0.05	0.09	0.01	0	0.14	0.08	0.01	(Dang et al., 2018)
41	Lake Chang	30.44	112.45	0.05	0.06	0.01	0.01	0	0	0.14	0.18	0.11	0.08	0.01	0	0.18	0.14	0.03	(Dang et al., 2018)
42	Lake Changdang	31.63	119.57	0.05	0.05	0.01	0.01	0	0	0.19	0.12	0.12	0.04	0.01	0	0.21	0.15	0.03	(Dang et al., 2018)
43	Lake Chao	31.57	117.67	0.05	0.04	0.01	0.01	0	0	0.19	0.1	0.11	0.06	0.01	0.01	0.22	0.16	0.03	(Dang et al., 2018)
44	Lake Dongping	35.96	116.2	0.06	0.07	0.01	0.01	0	0	0.17	0.16	0.12	0.05	0.01	0	0.18	0.13	0.02	(Dang et al., 2018)
45	Lake Dushan	35.08	116.77	0.06	0.09	0.01	0.01	0	0	0.15	0.19	0.09	0.06	0.01	0	0.2	0.11	0.02	(Dang et al., 2018)
46	Lake Gaoyou	32.82	119.35	0.05	0.06	0.01	0.01	0	0	0.15	0.12	0.1	0.1	0.01	0.01	0.19	0.15	0.03	(Dang et al., 2018)
47	Lake Hengshui	37.63	115.62	0.07	0.1	0.01	0.02	0	0	0.15	0.19	0.07	0.07	0	0	0.2	0.1	0.01	(Dang et al., 2018)
48	Lake Hong	29.9	113.4	0.05	0.08	0.01	0.01	0	0	0.14	0.16	0.11	0.06	0.01	0	0.21	0.13	0.02	(Dang et al., 2018)
49	Lake Hongze	33.31	118.75	0.05	0.06	0.01	0.02	0	0	0.13	0.11	0.1	0.12	0.01	0.02	0.17	0.16	0.04	(Dang et al., 2018)
50	Lake Hulun	48.95	117.39	0.06	0.17	0	0.01	0	0	0.09	0.28	0.04	0.1	0	0.01	0.15	0.07	0.01	(Dang et al., 2018)
51	Lake Liangzi	30.23	114.6	0.06	0.04	0.01	0.01	0	0	0.18	0.12	0.11	0.05	0.01	0	0.22	0.16	0.03	(Dang et al., 2018)
52	Lake Longgan	29.92	116.11	0.04	0.04	0.01	0.01	0	0	0.17	0.11	0.09	0.06	0.01	0.01	0.26	0.16	0.03	(Dang et al., 2018)

53	Lake Luoma	34.07	118.16	0.05	0.1	0.01	0.01	0	0	0.13	0.23	0.08	0.08	0.01	0	0.2	0.1	0.01	(Dang et al., 2018)
54	Lake Qinghai 1	36.86	100.31	0.08	0.19	0.01	0.01	0	0	0.1	0.22	0.04	0.06	0.01	0	0.21	0.07	0.01	(Dang et al., 2018)
55	Lake Qinghai 2	36.73	100.31	0.07	0.2	0.01	0	0	0	0.08	0.22	0.04	0.05	0.01	0.01	0.25	0.06	0.01	(Dang et al., 2018)
56	Lake Shijiu	31.5	118.94	0.05	0.07	0.01	0.01	0	0	0.17	0.14	0.11	0.05	0.01	0	0.21	0.15	0.03	(Dang et al., 2018)
57	Lake Weishan	34.61	117.26	0.06	0.07	0.01	0.01	0	0	0.18	0.15	0.11	0.05	0.01	0	0.2	0.12	0.02	(Dang et al., 2018)
58	Lake Wolong	42.75	123.29	0.09	0.14	0	0.01	0	0	0.18	0.25	0.04	0.07	0	0	0.15	0.07	0.01	(Dang et al., 2018)
59	Lake Wuchang	30.27	116.69	0.04	0.03	0.01	0	0	0	0.18	0.1	0.11	0.05	0.01	0	0.25	0.18	0.03	(Dang et al., 2018)
60	Lake Yangcheng	31.43	120.8	0.06	0.06	0.01	0.01	0	0	0.19	0.12	0.12	0.05	0.01	0	0.21	0.14	0.02	(Dang et al., 2018)
61	Lake zhenzhu	41.74	122.86	0.08	0.08	0	0	0	0	0.17	0.25	0.06	0.04	0.01	0	0.19	0.1	0.02	(Dang et al., 2018)
62	Longquanlongwan	42.42	126.6	0.04	0.06	0	0.01	0	0	0.19	0.18	0.05	0.06	0.01	0	0.3	0.09	0.01	(Dang et al., 2018)
63	Namtso 1	30.72	90.64	0.04	0.29	0.01	0.08	0	0.08	0.03	0.09	0.02	0.15	0	0.13	0.04	0.02	0.02	(Dang et al., 2018)
64	Namtso 2	30.78	90.46	0.05	0.29	0.01	0.08	0	0.07	0.03	0.1	0.02	0.15	0	0.12	0.04	0.02	0.02	(Dang et al., 2018)
65	Nanlongwan	42.41	126.48	0.08	0.07	0	0.01	0	0	0.2	0.17	0.06	0.07	0.01	0	0.19	0.1	0.02	(Dang et al., 2018)
66	Wuliangsuhai	40.87	108.78	0.06	0.18	0.01	0.02	0	0	0.06	0.29	0.04	0.12	0	0	0.15	0.06	0	(Dang et al., 2018)
67	Xidayang	38.75	114.77	0.04	0.09	0.01	0.02	0	0	0.11	0.26	0.05	0.09	0	0	0.2	0.1	0.01	(Dang et al., 2018)
68	Yuqiao	40.03	117.52	0.08	0.1	0.01	0.01	0	0	0.15	0.21	0.08	0.06	0.01	0	0.18	0.1	0.01	(Dang et al., 2018)

Table S2. The parameters for the lake model setup and references used to constrain the parameters.

Parameter	Value	Reference
Obliquity	23.4°	-
Latitude	33.39° N	Li *et al.* (2019)
Longitude	79.37° E	Li *et al.* (2019)
Local time (GMT)	+6	-
Maximum lake depth (m)	20	Li *et al.* (2019)
The elevation of the basin bottom (m a.s.l.)	4358	Li *et al.* (2019)
Area of the drainage basin (hectare)	38400	Li *et al.* (2019)
The neutral drag coefficient	0.002	Longo *et al.* (2020)
Shortwave extinction coefficient (1/meters)	0.3	Hutter *et al.* (2014) $\varepsilon = 1.1 * Zs^{-0.73}$; Zs = 6m, ε is Shortwave extinction coefficient; Zs is Secchi depth.
Fraction of advected air	0.3	Longo *et al.* (2020)
Albedo of melting snow	0.4	Longo *et al.* (2020)
Albedo of non-melting snow	0.7	Longo *et al.* (2020)
Salinity (ppt)	0.15	Li *et al.* (2019)

Table S3. Comparison of lake model simulated results with available observational data from western Tibet.

Name	Physical properties					Surface temperature (°C)					Ice cover	
	Type	Lat. (° N)	Lon. (° E)	Alt. (m a.s.l)	Max depth (m)	Spring	Summer	Autumn	Winter	MAT	Duration	Ice-out
Xiada Co	lake	33.39°	79.37°	4359	20	3.37	12.09	7.64	1.82	6.23	Dec. – Apr.	late Ap (avg. 19 Apr,)
Bangong Co	lake	33.5°	79.5°	4224	42.6	4.80	13.55	10.86	1.99	7.42	Dec. ~ Apr.	Apr
NASDE	station	33.39°	79.7°	4264	-	1.18	13.18	2.26	-10.08	1.64	N/A	N/A

Figure S1

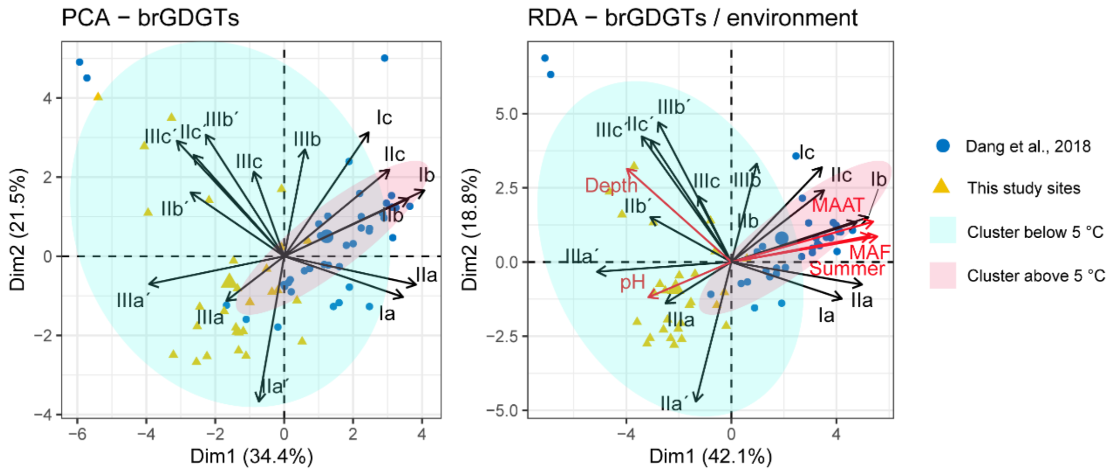

Figure S1. The principal component analysis (PCA) and redundancy analysis (RDA) for brGDGTs in our expanded lake surface dataset and previously published Chinese surface dataset (Dang *et al.*, 2018). The blue dots indicate the sites with MAAT above 5 °C and the yellow triangles represent sites with MAAT below 5 °C (a & b).

Figure S2

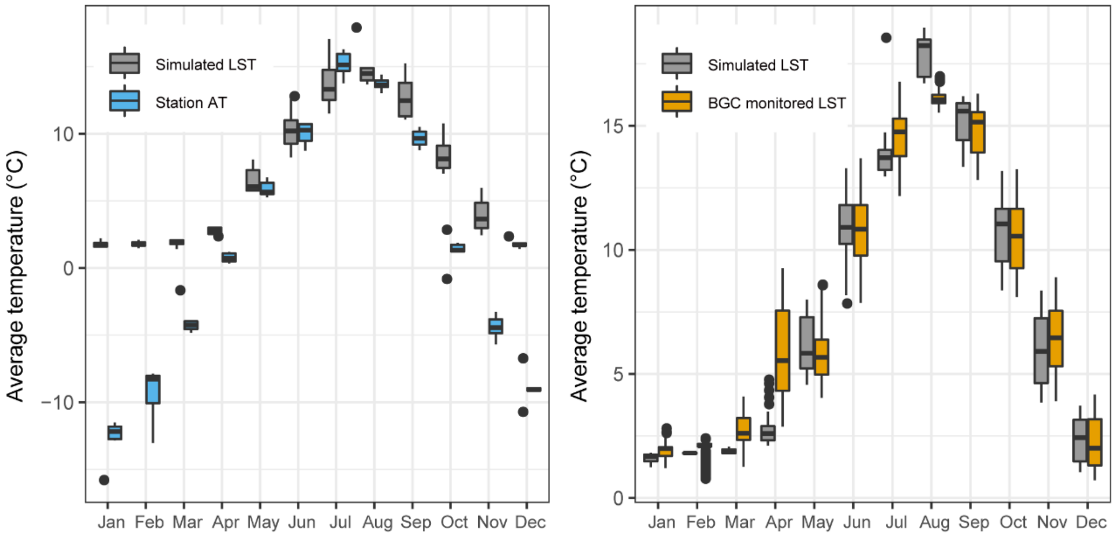

Figure S2. Comparison of (a) simulated lake surface water temperatures (above 5 m) for XDC (gray) and air temperatures from a nearby meteorological station (blue) for the period of 2010/1/1-2015/12/31; (b) comparison of simulated 5 m water temperature for XDC (gray) and monitored 5 m water temperature for BGC (yellow) for the period 2012/7/31-2013/7/30.

Figure S3

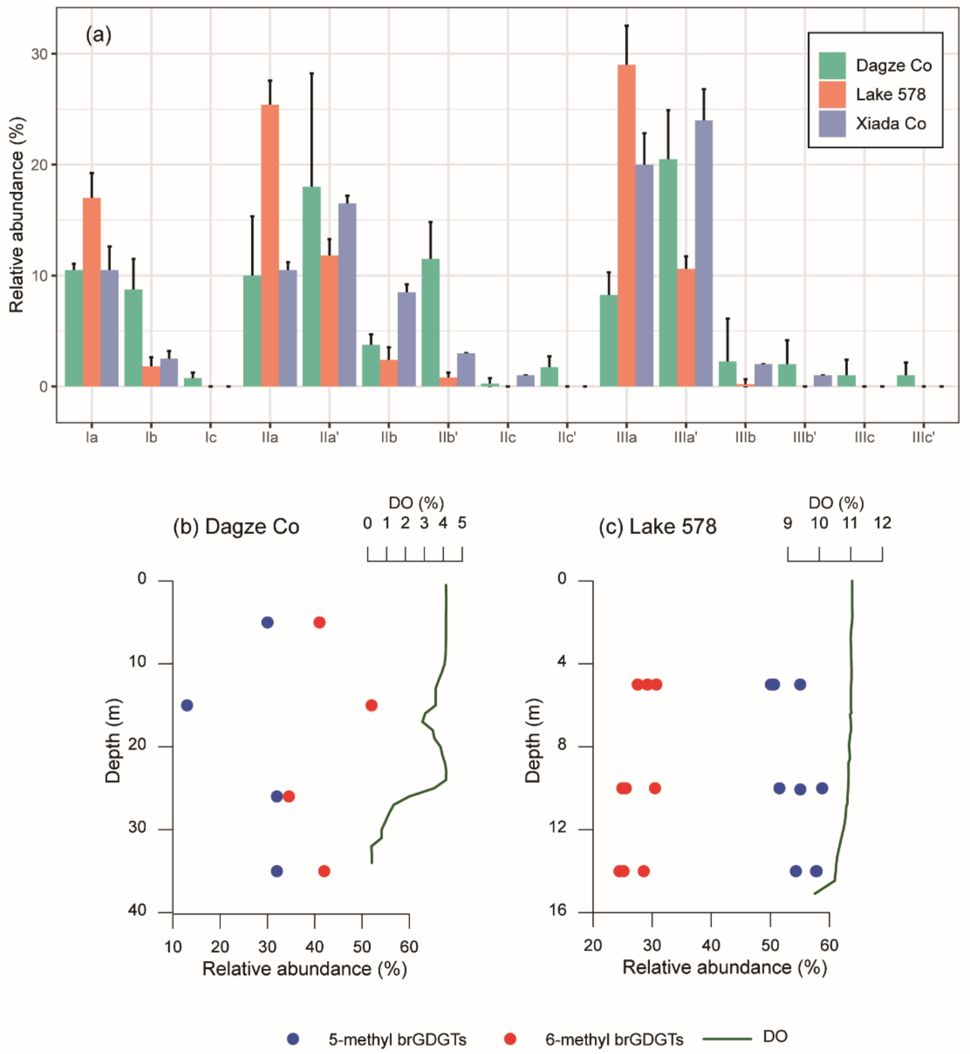

Figure S3. (a) Relative abundances of 5-methyl and 6-methyl branched tetraethers relative to total brGDGTs in surface sediments from Dagze Co, Lake 578 and Xiada Co. Reconstructed brGDGT compounds and temperature of (b) Dagze Co with (c) Lake 578 according to Zhao *et al.* (2021) are plotted 5- (IIa, IIb, IIc, IIIa; blue dots), 6-methyl (IIa´, IIb´, IIc´, III´a; red dots) brGDGTs related to MBT'_{6Me} and dissolved oxygen (DO).

Figure S4

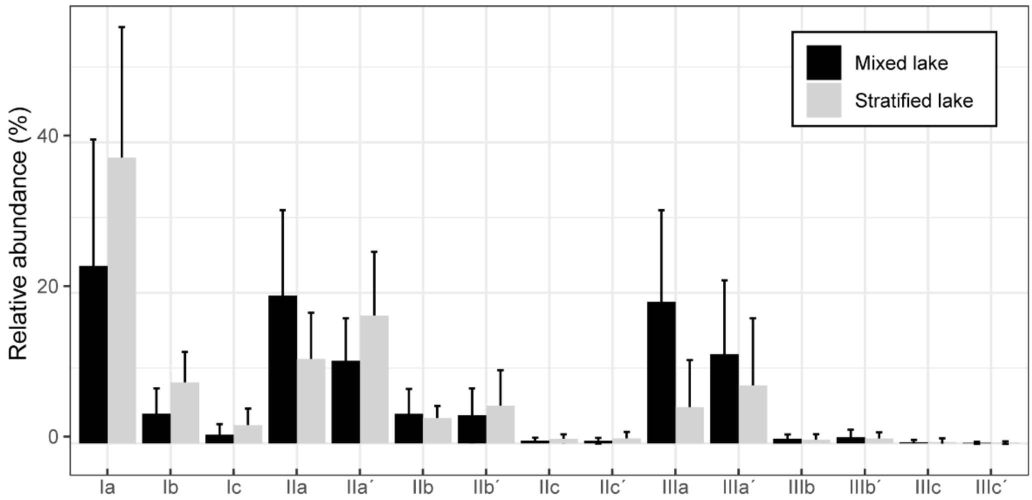

Figure S4. Relative abundances of 5-methyl and 6-methyl brGDGTs in surface sediments from mixed lakes and stratified lakes from ours and the global dataset (Martínez-Sosa *et al.*, 2021). The mixed lakes include Flatworm Lake, Robe Lake, Lago de Sanabria, Laguna Amarga, Lago Grande Estana, Mother Goose Lake, Allison Lake, Bangong Co, Lake 578 and Xiada Co. Stratified lakes include Big Soda Lake, Lake Malawi (LS21), Lake Kivu, Lake Malawi (LS28), Deming Lake, Crater Lake, Lake Edward, Big Croc Lake, Lake Malawi (LS48), Hot Water Lake and Dagze Co.

Figure S5

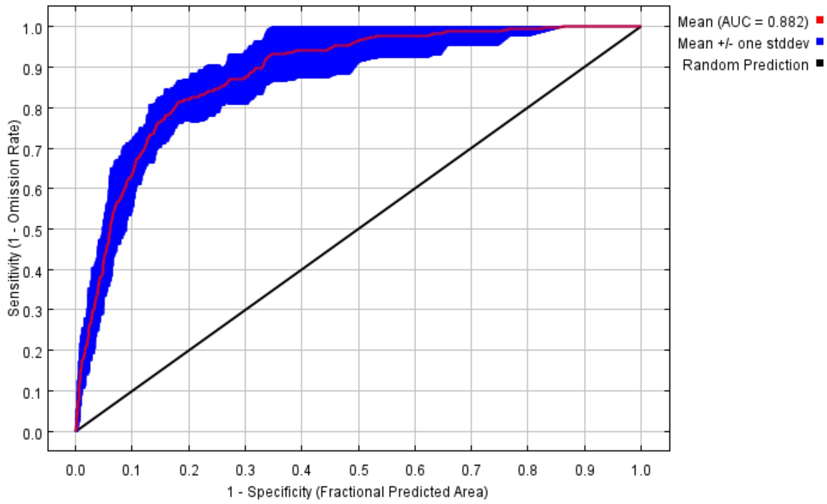

Figure S5. Extrinsic receiver operating characteristic (ROC) curves for MaxEnt on the distribution of Qingke barley (*Hordeum vulgare* L.).

Figure S6.

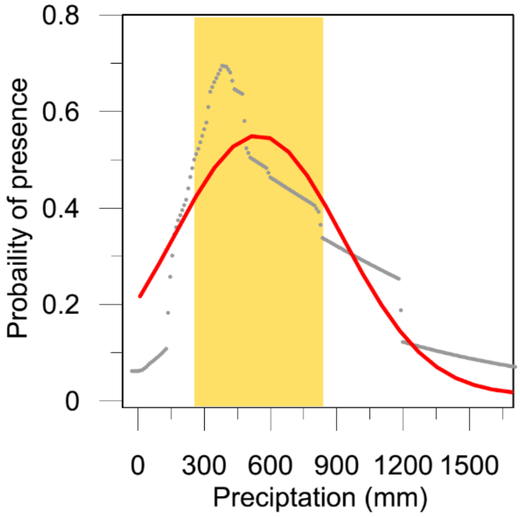

Figure S6. The optimal precipitation range for Qingke barley simulated by ecological niche modelling (MaxEnt model).

References

Dang, X., Ding, W., Yang, H., Pancost, R. D., Naafs, B. D. A., Xue, J., Lin, X., Lu, J., and Xie, S. (2018), Different temperature dependence of the bacterial brGDGT isomers in 35 Chinese lake sediments compared to that in soils. *Organic Geochemistry*, *119*, 72-79. https://doi.org/10.1016/j.orggeochem.2018.02.008.

Hutter, K., Chubarenko, I. P., and Wang, Y. (2014), *Physics of Lakes: Volume 3: Methods of Understanding Lakes as Components of the Geophysical Environment*. Heidelberg: Springer.

Li, X., Wang, M., and Hou, J. (2019), Centennial-scale climate variability during the past 2000 years derived from lacustrine sediment on the western Tibetan Plateau. *Quaternary International*, *510*, 65-75. https://doi.org/10.1016/j.quaint.2018.12.018.

Longo, W. M., Huang, Y., Russell, J. M., Morrill, C., Daniels, W. C., Giblin, A. E., and Crowther, J. (2020), Insolation and greenhouse gases drove Holocene winter and spring warming in Arctic Alaska. *Quaternary Science Reviews*, *242*, 106438.

Martínez-Sosa, P., Tierney, J. E., Stefanescu, I. C., Dearing Crampton-Flood, E., Shuman, B. N., and Routson, C. (2021), A global Bayesian temperature calibration for lacustrine brGDGTs. *Geochimica et Cosmochimica Acta*, *305*, 87-105. https://doi.org/10.1016/j.gca.2021.04.038.

Wang, M., Hou, J., Lazhu, Li, X., Liang, J., Xie, S., and Tang, W. (2021), Changes in the lake thermal and mixing dynamics on the Tibetan Plateau. *Hydrological Sciences Journal*, *66*(5), 838-850. https://doi.org/10.1080/02626667.2021.1887487.

Zhao, B., Castañeda, I. S., Bradley, R. S., Salacup, J. M., de Wet, G. A., Daniels, W. C., and Schneider, T. (2021), Development of an in situ branched GDGT calibration in Lake 578, southern Greenland. *Organic Geochemistry*, *152*, 104168. https://doi.org/10.1016/j.orggeochem.2020.104168.